Russian Chemical Reviews **79** (8) 693 – 712 (2010) © 2010 Russian Academy of Sciences and Turpion Ltd

DOI 10.1070/RC2010v079n08ABEH004108

Certain aspects of the formation and identification of nanosized oxide components in heterogeneous catalysts prepared by different methods

O G Ellert, M V Tsodikov, V M Novotortsev

Contents

I.	Introduction	693
II.	Methods of synthesis of nanostructured catalysts based on porous complex oxides	694
III.	Polymorphism of active phases and catalytic properties of nanostructured TiO_2 and mixed oxides on its basis	695
IV.	Polymorphism in metal oxide catalysts containing metastable phases	697
V.	Nanosized iron-containing complex oxide catalysts synthesized by the alkoxy method	701
VI.	The effect of the size factor on the catalytic properties of iron oxide catalysts on porous supports	705
VII.	Conclusion	708

Abstract. The results of studies into the relationship 'methods and synthesis conditions of a catalyst → catalyst structure → catalytic properties' in highly efficient crystallographically amorphous copper- and iron-containing heterogeneous systems obtained by different chemical methods are generalized. Polymorphism of active phases and catalytic properties of nanostructured copper-containing zinc, zirconium, manganese and cerium oxides are discussed. Unusual transformations of nanosized Pt- and Pd-containing components on the γ-Al_2O_3 surface in nanostructured catalysts of ethanol steam reforming into synthesis gas and reductive dehydration of ethanol to alkanes are considered. The results of comparative studies on the crystallographically amorphous mixed iron oxide catalysts synthesized by either the alkoxy method or the deposition on various supports obtained by the Mössbauer and XAFS spectroscopy and magnetic susceptibility measurements are presented. These materials are shown to be efficient catalysts of important processes such as liquid-phase oxidation of hydrocarbons, synthesis of alkenes and alkylaromatic hydrocarbons from CO and H_2, hydrogenative transformation of brown coal organic mass to hydrocarbons. The bibliography includes 242 references.

O G Ellert, V M Novotortsev N S Kurnakov Institute of General and Inorganic Chemistry, Russian Academy of Sciences, Leninsky prosp. 31, 119991 Moscow, Russian Federation. Fax (7-495) 954 12 79, tel. (7-495) 633 85 46, e-mail: ellert@igic.ras.ru (O G Ellert), tel. (7-495) 952 02 24, e-mail: vmnov@igic.ras.ru (V M Novotortsev)
M V Tsodikov A V Topchiev Institute of Petrochemical Synthesis, Russian Academy of Sciences, Leninsky prosp. 29, 119991 Moscow, Russian Federation. Fax (7-495) 954 22 92, tel. (7-495) 955 43 04, e-mail: tsodikov@ips.ac.ru

Received 5 October 2009
Uspekhi Khimii **79** (8) 758 – 779 (2010); translated by T Ya Safonova

I. Introduction

The EuropaCat-IX Congress held in Spain in 2009 came to the conclusion that 90% of the future progress of energy sources for the world chemistry complex will be based on catalytic processes. This is why attention was focused on the development of new-generation catalysts that should meet the following major demand: the active component structure should be controlled on the molecular and supramolecular levels in order to provide the high selectivity and activity in heterogeneous-catalytic reactions. This problem fully applies to industrial large-scale heterogeneous oxide catalysts. In the past 30 years, numerous publications appeared devoted to studies of the relationship 'methods and synthesis conditions of a catalyst → catalyst structure → catalytic properties'. The effect of both the nature of precursors (for instance, the type of metal-containing starting compounds, the nature and structure of supports, the use of templates, *etc*.) and the methods of synthesis of catalysts (impregnation, co-deposition, sol – gel process, *etc*.) on the composition, structural and size characteristics of the active components, their acid-base and electronic properties and operational stability are considered.

So far, virtually all industrial metal oxide catalysts were synthesized from aqueous solutions of metal-containing precursors (as a rule, inorganic salts), which by no means always provided the targeted formation of active components. The sol – gel process that employs metal alkoxides (the so-called alkoxy method or alkoxy synthesis) [1] as the reagents is the most promising method of targeted synthesis of complex oxides. Its main advantage is that it provides control over the hydrolysis and condensation steps and, as a consequence, the targeted formation of both molecular and supramolecular structures throughout the process. Particularly, the ions of foreign metals can be introduced into the growing partly hydrolysed structures from organic, *e.g*., acetylacetonate, complexes. In this case, heterometallic intermediates with the distances between atoms of different metals close to those in the final oxides could be developed in the step of amorphous gel formation.[2 – 4] The control over

the hydrolysis rate and the use of supercritical conditions and structure-forming additives allows one to affect not only the composition, the state of charge and the size characteristics of metal-containing active components but also the porous structure of the oxide as the whole. The targeted formation of the porous structure makes it possible to synthesize materials that behave as both membranes and catalysts.

In developing metal oxide catalysts, the important stage was the study of the genesis of the catalytic system in all steps of its formation. A particular difficulty in the study of the genesis is the presence of amorphous metal oxide components in the initial and sometimes final steps of the catalytic system formation. The advent of new accessible matter-research methods such as high-resolution scanning and transmission electron microscopy, X-ray absorption (EXAFS), the Raman and Mössbauer spectroscopy, magnetic methods allows one to follow the mechanism of transformations of the catalyst nanosized components in all steps of its synthesis, including *in situ* monitoring. The use of these methods makes it possible to study the fundamental electronic and structural characteristics of the catalytically active sites in mixed metal oxide catalysts and their interaction with the substrate.

To date, several reviews devoted to the spectroscopic methods of studies of nanostructured mixed metal oxides have been published (*e.g.*, see Refs 5, 6). The presence of magnetic metal ions in the oxide catalysts, particularly iron ions, made it possible to effectively use the Mössbauer spectroscopy and magnetic methods for precision control over the changes in the active site structures in crystallographically amorphous materials. Unfortunately, only few reviews are devoted to the use of the Mössbauer spectroscopy in catalysis. Moreover, these studies mainly considered the catalysts for the Fischer–Tropsch and ammonia synthesis.[7–12]

For a long time, studies have been carried out in the field of alkoxy synthesis of mixed metal oxide catalysts from homo- and heteronuclear metal acetylacetonates (particularly, copper and iron complexes) for several important petrochemical reactions. This is the subject of many publications, however no reviews have been published.

Recently, metal oxide catalysts have become the matter of keen attention, which was associated with their wide use in several important catalytic processes, for instance, methanol steam reforming. Numerous methods for the synthesis of these catalysts (including the sol–gel method) were developed that allowed modifying their structures and improving their operational characteristics.

The goal of the present review was the generalization of results of studies on the formation of nanosized active oxide components in crystallographically amorphous copper- and iron-containing heterogeneous systems prepared by the alkoxy method and their evolution throughout the reaction. The formation of active nanocomponents, from the initial step of their nucleation through the preactivation step up to the *in situ* reaction, is monitored using the Mössbauer spectroscopy, EXAFS, magnetic susceptibility and magnetization methods. The review also presents new data on nonequilibrium interactions of noble metal clusters with the surface ions of the oxide carrier. This review does not consider zeolite catalysts, because this broad theme has already been thoroughly discussed in several recent reviews.[13–16]

II. Methods of synthesis of nanostructured catalysts based on porous complex oxides

Porous mixed oxides pertain to compounds often used in heterogeneous catalysis. This is associated with the power-saving reactions involved in their synthesis, which occur under mild conditions. The large number of diverse precursors, additives and modifiers and the possibility of varying the thermal treatment conditions provided wide opportunities for the development of metal oxide catalysts with the desired chemical composition, microstructure, porosity and surface properties. Metal oxides are the components of virtually all industrial catalysts as either their active phase, or additives, or supports.

Porous metal oxide catalysts including nanostructured ones are synthesized by different chemical methods such as co-deposition of colloids,[17–19] the impregnation method,[17–20] the aerosol method,[20] the method of hydrodynamic cavitation,[21,22] the ultrasonic method,[23,24] the surface self-propagating thermal synthesis,[25,26] the sol–gel process,[1–4] *etc*. Each of them requires its own, the most efficient catalyst.

Specific procedures are to be developed for the preparation of a given catalyst that represent certain modification of a standard protocol for synthesizing this class of compounds. Such modifications involve changes in any parameter of the standard method, for example, concentration, the type of metal-containing precursor, the nature of additives, the temperature mode, the sequence of steps, *etc*. Although the procedures presented in original publications are referred to as the standard methods, they include details that transform them into individual modified versions of the known method. Insofar as the detailed description of procedures reported in each cited study would convert our review into a voluminous manuscript, we decided to mention the methods only under their original names in hope that the interested reader will easily find all details in the cited publications.

Nanoparticles of metal oxides, especially mixed oxides, can exhibit unique chemical properties due to their small sizes and high density of active surface sites formed by angles and faces of nanostructures.[7] The main goal in designing nanosized metal oxide catalysts is to control their grain size and morphology. For this a synthetic method is the preferred choice as it successfully achieves both of these conditions and determines the catalysts structure, which in turn determines the properties of the overall catalytic system.[27] Many examples are known (*e.g.*, see Refs 28–30) where mixed oxide catalysts with the same composition but obtained by different methods exhibited different activity. The examples are shown in the subsequent text.

Thus micelles (microreactors) are used in the colloid method in which the solvated metal cations react with the precipitant ions. This is considered[17–19] as the most efficient known method in achieving high dispersion, uniform distribution of mixed metal oxides over the bulk and narrow size distribution of particles. Moreover, under conditions of the colloidal synthesis, the targeted development of a wide spectrum of structures and grain sizes is possible.[31,32]

However, from our viewpoint and also in the opinion of authors of several reviews,[2–4] the sol–gel method is the most suitable for preparing highly dispersed heterogeneous catalysts based on porous complex oxides. The advantage of this method is that it allows one to control the formation of

ultrafine highly chemically homogeneous powders and also that power consumption in this process is low.

To date, the sol–gel process became almost a standard method of targeted synthesis of nanosized catalytic systems used in structure-sensitive reactions. This process is based on the hydrolysis of mono- and heterometallic precursors often containing organic ligands. The use of organic groups in the construction of purely inorganic sol–gel materials makes it possible to control the reaction rates of precursors, the rheology of sols and the homogeneity and microstructure of the synthesized gels. Back in the 1980s, it was noted that metal oxides synthesized by the sol–gel method from metal alkoxides as the starting materials were the systems with higher dispersion as compared with oxides prepared by hydrolysis of inorganic salts of the metals in aqueous solutions.[33,34] It was demonstrated that many metal chelate complexes react with alkoxide complexes to form mixed metal oxides with the clearly pronounced microstructure uniformly distributed throughout the volume. Based on indirect data, it was assumed that in the course of the alkoxy synthesis† of complex metal oxides, the ligand exchange could occur even in mother solutions.[35–39] These assumptions were confirmed by an X-ray diffraction study[40] of a single crystal of a mixed metal-oxide intermediate synthesized by the reaction of tetra(n-propoxy)zirconium with iron(III) acetylacetonate. It was shown that the ligand exchange led to coordination of acetylacetonate ligands to zirconium(IV) ions in the single crystal, while alkoxide ligands were coordinated to iron(III) ions.

Recently, a new method of synthesis of metal oxide catalysts based on the so-called surface self-propagating thermal synthesis has been developed. This method results in formation of non-equilibrium highly dispersed oxide phases of high defectiveness on the surface of the oxide support.[25,26] The active phase formation on the support surface occurred in the combustion wave of interacting metals supported on the surface from their organic salts. The highly dispersed oxide phases formed in the exothermic reaction occupied the support surface. It was shown that the thus synthesized catalysts based on rare-earth metal oxides exhibited high activity in cleaning the exhausts of internal combustion engines in the so-called 'three-way' catalytic process (including the following three reactions: oxidation of CO and hydrocarbons and reduction of NO).

III. Polymorphism of active phases and catalytic properties of nanostructured TiO_2 and mixed oxides on its basis

The synthesis of mesoporous titanium dioxide (TiO_2, titania) is often carried out by the sol–gel method. It is known that the ionization energy of TiO_2 in the form of anatase is 3.2 eV, which makes this material an ideal candidate for the use in UV-induced photochemical processes. The other advantages of titania are its cheapness, safety, chemical and biological neutrality and stability. This makes it the most promising catalyst in many photochemical processes such as CO_2 photoreduction, photooxidation of volatile organic compounds (VOC), *etc.*[41–44]

† The sol–gel methods for the synthesis of complex metal oxides from metal alkoxides as the starting compounds are referred to as the alkoxy syntheses or alkoxy methods.[1]

The synthesis of TiO_2 by the sol–gel method from titanium-containing organic or inorganic precursors is carried out in the presence of surfactants and stabilizing agents.[45–53] This synthesis results in titanium dioxide as a porous gel, which is transformed to oxide by thermal treatment.[53] In the majority of cases, the thus prepared mesoporous titanium oxide is either crystallographically amorphous or polycrystalline with the amorphized structure. Although further heating at high temperatures leads to its crystallization, the excess thermal energy often brings about collapse of mesopores, which is accompanied by the decrease in both the specific surface and the volume of the adsorption pores.[53,54] Thus, the low-temperature synthesis of mesoporous titania with the crystalline structure is so far a challenge.

In a study[44] aimed at elucidation of how the surface structure of titana affects its photocatalytic properties, the synthesis of titania was carried out by a modified sol–gel method that included precipitation of an amorphous titanium dioxide gel followed by controlled crystallization under different conditions. In this way, crystalline monodisperse nanostructured anatase TiO_2 samples were produced as well as crystalline aggregates of these samples with the anatase structure, too. The crystallinity, size and phase composition of TiO_2 nanograins and also the size and the shape of their aggregates were shown to depend on the crystallization conditions (thermal and hydrothermal processes and outgassing in dry air under UV irradiation). By varying the crystallization conditions, the structure and the degree of surface hydration of TiO_2 samples could be controlled, which substantially affected their photocatalytic activity. Thus, by the example of the TiO_2-catalyzed reaction of trichloroethylene photooxidation, it was found that the hydroxyl groups of low-coordinated titanium atoms were responsible for the generation of by-products, namely, dichloroethylene and dichloroacetaldehyde, which reduced the conversion of trichloroethylene and sometimes led to catalyst deactivation. Moreover, the inverse dependence of the titania catalyst efficiency in the mineralization reaction on the irradiation energy and the number of surface defects was inferred.

The synthesis of silica-supported titania catalysts (TiO_2/SiO_2) was described.[54] Samples were prepared by grafting tetra(isopropoxy)titanium, $Ti(OPr^i)_4$, onto silica. This method led to formation of strong Si–O–Ti bonds, which are responsible for the high degree of titanium dioxide dispersion. At a low Ti loading, titanium dioxide polyhedra with tetrahedral configuration formed on the catalyst surface until the maximum surface monolayer coating ($\sim$2.2 Ti atoms per nm^2) attained. The increase in the TiO_2 surface concentration gave rise to titanium ions with octahedral environment. Such a change in the geometry of surface active sites had a substantial effect on the catalytic properties of TiO_2/SiO_2 samples. It was found that the activity and selectivity of silica-supported titania catalysts in the reaction of cyclooctene epoxidation with cumene hydroperoxide is inversely proportional to the amount of grafted titanium dioxide, *i.e.*, it is the titanium ions in the tetrahedral environment that are the active sites of this reaction.

The ability of mixed oxides to form uniform porous structures was first demonstrated in 1970.[55] It was concluded that self-organization involved not only the structure but also its defects, which were subsequently named Wadsley's defects. Later it was found[56,57] that certain organic

phosphites added to solutions of titanium alkoxide in the alkoxy synthesis favour structuring of the resulting TiO_2 samples. The obtained single-phase oxides $P_xTi_{1-0.75x}O_{2\pm\delta}$ had a homogeneous pore structure and a narrow pore size distribution. It was found that the pore size in titania can be regulated in the range from 2 to 4 nm depending on the molecular volume of the phosphorus-containing precursor. This allowed development of catalytic systems with the molecular sieve properties [58] for the ethylene glycol oxyethylation to diethylene glycol. In addition, based on these oxides, hybrid membrane-catalytic systems were developed [59] that exhibited not only selective permeability to gases but also anisotropy of catalytic activity in the methanol dehydrogenation reaction, which depended on the direction of the gaseous substrate flow. This opened up the possibility of developing a membrane-catalytic diode. The theoretical analysis [59] of independent models of gas diffusion through microchannels in such membranes containing nanosized catalytic systems made it possible to infer the increase in the lateral diffusion of gas molecules in the diffusion flow, which increased the probability of collisions of the gaseous substrate molecules with the active surface in the inner volume of membrane microchannels. The catalysis in membrane pores led to the increase in the mass and heat exchange, which favoured intensification of several catalytic reactions as compared with traditional catalysis in a reactor filled with a stationary catalyst layer.

One of the ways of increasing the quantum yield of titania photocatalysts was the introduction of defects into the titania matrix in the form of dopant ions of transition metals. Numerous studies were devoted to the use of titania as the support (commercial oxides manufactured by Degussa, Aldrich, Fuji Titan) in the synthesis of complex metal oxides or as a component of mixed oxides prepared by the alkoxy synthesis. Copper attracted attention as a dopant due to its cheapness, accessibility and catalytic activity in several important industrial reactions, for example, in the CO_2 reduction and NO_x decomposition, which allowed this metal to be considered as a candidate in the development of industrial catalysts devoid of noble metals. It was shown that doping of titania with copper(II) ions extends the light absorption to the visible region [60] and also improves its photocatalytic activity.[42, 61–64]

Several studies considered the effect of the preparation conditions of copper titanate ‡ catalysts on their structures and catalytic activity. Thus the structure of Cu/TiO_2 catalysts prepared by impregnation or chemisorption-hydrolysis methods of copper nitrate on commercial titanium oxide [65] was used in both cases as the copper-containing precursor. In these processes, the copper-containing surface layer was formed *via* different inorganic intermediates. Thus in the former case, the transformation of the copper-containing precursor into copper–titanium oxide proceeded *via* the monoclinic modification of $Cu_2(OH)_3NO_3$. Calcination of the latter afforded the crystallographically amorphous copper oxide phase. In the latter case, the aforementioned intermediate was not detected on the support surface and the resulting surface layer represented small CuO crystallites particles easily reducible to metallic copper.

‡ The term ‘titanate’ was used for complex oxides in which TiO_2 was the structural motif; the same meaning was put into the term ‘zirconate’.

The above information agrees with the data of a series of publications by Wu *et al.*[41, 42, 66, 67] These authors considered copper–titanium oxide catalysts prepared by different methods (impregnation and alkoxy synthesis) from different copper-containing precursors, namely, inorganic (copper chloride) and organic (copper acetate) one, and their use in the photocatalytic reduction of CO_2. It was assumed that the interaction of the Cu ions with the TiO_2 molecules was stronger in the Cu/TiO_2 catalysts synthesized by the sol–gel method as compared with impregnation method. The use of copper chloride as the precursor led to the stronger copper–titanium dioxide interaction § as compared with copper acetate, which was reflected in the higher photoactivity of the catalyst prepared from the inorganic copper-containing precursor.[42] It was thus concluded that individual nanosized particles containing Cu(I) ions are the active sites of the CO_2 catalytic photoreduction. The alkoxy synthesis employing copper chloride afforded less aggregated copper particles with Cu(I) active sites resistant to both thermal treatment and reduction with hydrogen, which makes both this method and this type of copper-containing precursor promising in preparing catalysts for CO_2 reduction.

The conclusion drawn by Wu *et al.*[42] on the effect of the nature of a copper-containing precursor agrees with the results of the other study [68] where the relationship ‘catalyst’s synthetic method and conditions → catalyst structure → catalyst properties’ was considered from the viewpoint of the effect of the nature of copper-containing precursor (copper chloride and sulfate) on the structure of the titania component of the Cu/TiO_2 catalysts prepared by the alkoxy synthesis. It was found that in the case of $CuSO_4$, the titanium dioxide component contained equal fractions of rutile and anatase phases, while for $CuCl_2$, it contained phases with the brookite and anatase structures. The differences in the titania phase composition determined the differences in their defects and hence the different strength of the copper–titanium dioxide interaction. Using the temperature-programmed reduction (TPR) method, it was found that the hydrogen consumption by a sample prepared from copper sulfate exceeded 20-fold that from copper chloride, which suggests the stronger $Cu-TiO_2$ interaction in the latter case.

Single-phase systems with the empirical formula $Cu_xTi_{1-0.5x}O_{2\pm d}$ and the anatase structure were synthesized [69, 70] by the alkoxy method from tetra(n-butoxy)titanium and copper stearate. These systems exhibited the high activity in low-temperature oxidation of carbon monoxide to carbon dioxide, comparable with the activity of industrial catalysts containing noble metals. It was found that for $x = 0.01-0.08$, Vegard’s law was obeyed, which pointed to the formation of single-phase oxides in this concentration range. The increase in the number of copper ions involved in the anatase structure within the limits of the single-phase state of the system was accompanied by an increase in the degree of dispersion of microcrystallites up to 6–8 nm and, as a consequence, the increase in the catalytic activity. An attempt to further increase the copper content ($x > 0.08$) led

§ The term ‘strong interaction metal–support’ was originally introduced for characterizing the interaction between the coordinatively unsaturated highly dispersed active phase and a metal oxide support in mixed catalysts [S Tauster, S C Fung, R T K Baker, J A Horsley *Science* **211** 1121 (1981)]

to abrupt heterogenization of the system with coarsening of microcrystallites and the formation of rutile and copper oxide phases measuring no less than 15–20 nm.[70] The phase heterogenization of the system was accompanied by the loss of catalytic activity.

IV. Polymorphism in metal oxide catalysts containing metastable phases

Based on experimental data and theoretical calculations, an important conclusion was drawn that the main criterion in the formation of the phase composition of metal oxide crystallites was the surface free energy rather than the volume energy.[71] This is the rationale for the fact that many nanostructured materials are formed as metastable phases. Phase transformations of catalyst's active components depend on the synthesis conditions. For example, the aerosol synthesis of $Cu_xZn_{1-x}Cr_2O_4$ oxides afforded nanostructured metastable crystallites with the cubic spinel structure in all series of samples with the substitution x up to 0.90, in contrast to other methods used for synthesizing these oxides, which produced mixed oxides with the stable tetragonal structure.[72]

The simplified view on the role of support in complex oxide catalysts considered the support as an inert carrier of the oxide component. From this viewpoint, the support affected only the size and thermal stability of active metal particles. However, the latest research in this field clearly demonstrated the dependence of the catalytic activity of particles on the support type, the method of its preparation and structure.[73–80] Thus for copper-containing catalysts it was found that Cu-ZnO catalysts synthesized by the co-deposition method were more active in the methanol synthesis than supported Cu/ZnO catalysts obtained by impregnation.[78] Moreover, a comparison of Cu/ZnO and Cu/TiO_2 catalysts with the same dispersity of copper particles on the support surface has demonstrated the fundamental difference between the catalytic activities of the mentioned systems.[79] Interesting experimental data have been collected on the structural transformations that occurred in the interaction of 'catalytically active' copper with the oxide matrix, where the latter played the key role in the attainment of the optimal dispersion of copper and also in the maintenance of copper in this state.

For these reasons, it seems very important to consider the problem of polymorphism of active components in copper-containing catalysts prepared on different metal oxide supports.

1. Polymorphism of active phases and catalytic properties of nanostructured copper-containing zinc, zirconium, manganese and cerium oxides

a. Polymorphism of active components and catalytic properties of copper-containing catalysts based on ZnO

Methanol synthesis from the $CO-CO_2-H_2$ mixture is the most important industrial method that usually employs mixed copper–zinc oxides as the catalysts.[81–83] Numerous publications deal with the methanol synthesis (for example, see Refs 84–87). However, the opinions of scientists on the problems concerning the reaction mechanism, the role of ZnO and the structure of active sites of copper–zinc oxide catalysts were so far controversial. Thus there are two viewpoints on the nature of active sites. One of them states that the active sites in such catalysts are atoms of metallic copper;[88–93] the second assumes that the active sites represent the copper ions that interact with the oxygen ions in the zinc oxide support.[94–96] As regards the role of ZnO, the opinions are also contradictory. The following four hypotheses have been put forward: 1) the use of the ZnO support enhances the dispersity of copper;[88,89] 2) ZnO operates as the reservoir for hydrogen atoms that propagate over the copper surface and favour the hydrogenation process;[97–99] 3) ZnO determines the morphology of the copper particles by stabilizing the active planes;[100–102] 4) ZnO favours the formation of active sites on the Cu surface.[81,103–114] Whereas the first opinion is in fact generally accepted, there is no agreement as regards the rest three opinions. In connection with this, we believe that a series of publications[84–87] supplementing one another can bring certain clarity to these problems. In the aforementioned publications, the Cu–ZnO catalysts were synthesized by the co-precipitation method usually employed for this purpose in industry. The method consisted of mixing aqueous solutions of copper and zinc nitrates with aqueous solutions of Na_2CO_3 or $NaHCO_3$, which was followed by the precipitation of intermediates such as malachite $Cu_2CO_3(OH)_2$, aurichalcite $(Cu,Zn)_5(CO_3)_2(OH)_6$ or hydrocincite $Zn_5(CO_3)_2(OH)_6$. The co-pecipitation products were subjected to ageing and annealing and studied by different physicochemical methods. The following conclusions could be drawn. The data of scanning tunnelling microscopy[84] and EXAFS[86] suggested that on the Zn/Cu(111) plane, the surface Cu–Zn metal alloy formed, which was probably responsible for the formation of active sites. Reflection IR spectroscopic data obtained *in situ*[84] made it possible to elucidate the mechanism of active site operation and of the process as a whole. Particularly, it was found that the formate groups coordinated to active sites were easily hydrogenated to the methoxy groups. Thus, it was found that in addition to dispersing Cu over the support surface, the role of ZnO consisted of the formation of catalytic active sites, namely, a surface Cu–Zn metal alloy. In studying the effect of the nature of the precursor, it was found that aurichalcite is the ideal precursor because it contains a homogeneous mixture of the Cu and Zn ions. Studies by the X-ray diffraction method have revealed[85,86] how the ageing step and the molar ratio Cu : Zn affected the formation and the degree of deformation of copper crystallites. Structural defects in crystallites could be caused by penetration of ZnO into the latter or incomplete reduction of copper, which could result in deformation of the copper surface and thus affect its catalytic activity. It was shown that the changes in the microstructure of copper and ZnO crystallites (particularly, in the particle size, deformation, lattice parameters) correlated with the changes in the phase composition of hydroxycarbonate precursors. The catalytic activity of copper–zinc oxides with 60% Zn content was higher than that of analogous oxides with 30% Zn.

b. Polymorphism of active components and catalytic properties of copper-containing catalysts based on ZrO_2

Copper-containing catalysts are widely used in reactions of selective catalytic reduction of NO_x, water-gas conversion as well as in methanol synthesis and steam reforming.[85,115–125] The high selectivity of these catalysts was observed in reactions of furfural reduction to furfuryl alcohol, dimethyl ether conversion to methanol and hydrocarbons and also in alcohol oxidation to the corresponding aldehydes or ketones.[126–130] The catalysts used in these processes employed ZrO_2 as the support.[119,131–134] For

example, the addition of ZrO_2 to copper-containing Cu/SiO_2 or Cu/ZnO catalysts used in reactions of CO or CO_2 hydrogenation increased the stability, activity and selectivity of catalysts.[135–144] It was also found that the support structure had a substantial effect on the properties of the catalytic system. For example, Cu/ZrO_2 catalysts based on ZrO_2 with the monoclinic structure (m-ZrO_2) exhibited activity in the methanol synthesis approximately one order of magnitude higher than the catalyst with the same surface concentration of Cu on the ZrO_2 support with the tetragonal structure (t-ZrO_2),[145] the specific surfaces of m-ZrO_2 and t-ZrO_2 being equal. Presumably,[146, 147] the observed differences were due to the presence of the larger number of defects on the surface of m-ZrO_2 as compared with t-ZrO_2.

Let us consider this problem in more detail. Among the main three types of crystalline ZrO_2, namely, t-ZrO_2, m-ZrO_2 and cubic (c-ZrO_2), the catalytic properties of c-ZrO_2 has been least studied. This is associated first of all with the instability of this structure at room temperature.[148] In both cubic and tetragonal phases, each Zr ion is surrounded by eight oxygen anions that form two bound tetrahedrons in which each oxygen atom is connected with four neighbouring Zr atoms. Different deformation of the tetrahedra in the cubic and tetragonal phases results in different Zr—O and Zr—OH bond distances on the support surface. This is why the deformation of the [ZrO_8] structural fragment in t-ZrO_2 is more pronounced than in c-ZrO_2. In m-ZrO_2, the Zr ions are coordinated with seven oxygen atoms and form two types of non-equivalent oxygen sites.[149] The structural distortions in [ZrO_7] were the strongest among the given three allotropic phases, which was manifested by the non-equivalent nature of all seven Zr—O bonds. Presumably, it is the difference in the space symmetry of Zr—O and Zr—OH bonds on the support surface that determines the dispersity of active metal-containing components and hence the catalytic properties of mixed Cu/ZrO_2 oxide.[146, 150]

It was underlined[145–151] that the activity of Cu/ZrO_2 catalysts in methanol steam reforming crucially depends on the ZrO_2 phase structure. In this process, the retention of the amorphous zirconia structure in the calcination step and under the reaction conditions was the main prerequisite for reaching the high activity/selectivity and for increasing the stability of copper–zirconia catalysts. Yet another important aspect is the well developed surface at the copper/zirconia interface.[152]

The structural evolution of components in $Cu–ZrO_2$ systems was considered in detail[153] for the calcination step. Catalysts $Cu–ZrO_2$ were prepared by co-precipitation of copper and zirconium oxalates followed by drying the resultant gel and calcination. The structural changes were followed by X-ray powder diffraction (XRD) and visible Raman spectroscopy. It was found that phase evolution of the ZrO_2 matrix in a mixed copper–zirconium oxide follows the sequence of amorphous → tetragonal → monoclinic in the temperature range 350–750 °C. The results of XRD studies showed that the conversion of the tetragonal phase into monoclinic started at 650 °C and completed at 750 °C. At the same time, according to Raman spectra, the transformation of the tetragonal phase into monoclinic started already at 550 °C. This suggests that the phase transformation initially occurred at the surface layer of copper–zirconia and then in its bulk. The phase transformations on the catalyst surface resulted in the formation of anionic defects due to the appearance of structural fragments containing Zr^{3+} ions, as detected by X-ray photoelectron spectroscopy. Earlier,[154] based on the data of surface-enhanced UV Raman spectroscopy, it was shown that the transformation of the tetragonal phase of ZrO_2 to the monoclinic phase during the calcination started from the surface and propagated into the bulk. This process began at 400 °C and completed at 700 °C. A comparison of XRD data and visible Raman spectra[153] for the mixed oxide $Cu–ZrO_2$ with the data from UV Raman spectroscopy[154] for t-ZrO_2 showed that the transformation of the tetragonal ZrO_2 phase into the monoclinic phase in the mixed oxide $Cu–ZrO_2$ required higher temperatures as compared with t-ZrO_2. This was explained[153] by stabilization of the metastable tetragonal zirconium oxide structure by copper ions in the surface layer. Thus, the zirconium dioxide structure plays an important role in establishing the relationship between the structure and the catalytic activity of copper–zirconium oxides.

Yet another factor that affected the activity of mixed $Cu–ZrO_2$ catalysts was copper specific surface.[153] The changes in the catalytic activity of copper–zirconium oxides in steam reforming were analyzed as a function of the calcination temperature. No linear correlation was observed between the increase in the rate of H_2 formation and the increase in the specific surface of copper for catalysts under consideration, which made it possible to infer the necessity of taking into account the strong copper–zirconia interaction. From our viewpoint, this means that it is the highly dispersed CuO phase that is responsible for the activity of these materials. Indeed, the results of TPR showed that in the material under study, at least three types of CuO components were present. These are the highly dispersed CuO phase, crystalline copper oxide and also individual Cu(II) ions incorporated in a complex oxide. The latter represented the monoclinic zirconia phase enriched in copper in its surface layer. Probably, it is this phase that is the most active in methanol steam reforming catalyzed by the described systems.

c. Polymorphism of active components and catalytic properties of copper-containing catalysts based on MnO_x

Mixed copper–manganese oxide catalysts were also applied in certain industrially important processes such as CO oxidation,[155, 156] low-temperature NO reduction,[157] water-gas shift reaction,[158] VOC processing[159] and other hydrogenation and oxidation reactions.[160–164] In addition, these oxides exhibited high catalytic activity in methanol steam reforming, which could be an alternative to the conventional catalytic synthesis of high-grade hydrogen for fuel cells.[165–167]

Numerous publications are devoted to synthetic methods, structure and properties of mixed copper–manganese oxides. It is assumed that copper–manganese components with the spinel structure resulting from a strong $CuO–MnO_x$ interaction are the active elements of these systems.[168] The enhanced catalytic activity of copper–manganese oxides is believed to be associated with the non-stoichiometric spinel phase.[158, 159, 167–169] At present, the synthesis of copper–manganese oxides can be carried out by several methods of which the co-precipitation of metal hydroxycarbonates is the most popular. However, a comparative analysis[170] revealed certain drawbacks of this method, particularly, the necessity of calcination at a temperature above 500 °C for crystallization of a phase

with the spinel structure, which is the reason for the undesired sintering and the dramatic decrease in the specific surface. The formation of large amounts of liquid and gaseous wastes places this reaction among processes that consume large amounts of energy and present environmental problems. In a series of publications [170–174] devoted to the synthesis of copper-containing oxide catalysts by the mechanochemical method, the prospects of this approach as compared with the standard co-precipitation were demonstrated. In the proposed method, grinding of a mixture of solid starting compounds, namely, $Cu_2CO_3(OH)_2$, $MnCO_3$ and an excess of oxalic acid, in a planetary mill was followed by calcination at different temperatures. The effects of the nature of metal-containing precursors, the milling intensity and the calcination temperature on the catalytic activity, selectivity and stability of final mixed oxides in the test reaction of methanol steam reforming was studied in detail. The structure and porosity of synthesized samples were examined invoking the N_2 adsorption, X-ray diffraction, diffuse reflectance IR Fourier transform spectroscopy (DRIFTS) and TPR methods. The XRD studies revealed the presence of the $Cu_{1.5}Mn_{1.5}O_4$ mixed oxide with the spinel structure, which is a non-stoichiometric form of $CuMn_2O_4$. It should be noted that the mixed oxide was formed at the calcination temperature of 300 °C, whereas in samples synthesized by co-precipitation, this occurred at a higher temperature (> 500 °C). According to the TPR data, the prepared catalysts represented mixtures of several phases, which included the non-stoichiometric oxide $Cu_{1.5}Mn_{1.5}O_4$ with the spinel structure, crystalline CuO as well as MnO_x interacting with $Cu_{1.5}Mn_{1.5}O_4$. It was shown that the catalytic activity of mixed oxides synthesized by the mechanochemical method substantially depended on the nature of precursors and also on the intensity of grinding. For example, a mixed oxide sample prepared from oxalate precursors proved to be more active than a sample synthesized from citrate precursors. Thus methanol was converted by 92% at 240–260 °C in the presence of the former catalytic system and by 68% in the presence of the latter system. Moreover, it is evident that samples calcined at 300 °C exhibited higher activity as compared with samples calcined at 500 °C. The higher activity of a catalyst synthesized at 300 °C was attributed to the formation of grains with the predominant content of the catalytically active $Cu_{1.5}Mn_{1.5}O_4$ spinel phase. The latter was characterized by the high specific surface and the small size of copper oxide nanocrystals, which resulted in their stronger interaction with the support phase. The catalytic properties of mixed copper–manganese spinels synthesized by conventional co-precipitation were much inferior.[166, 167]

d. Polymorphism of active components and catalytic properties of copper-containing catalysts based on CeO_2

The use of ceria in industrial heterogeneous catalysis is owed to its high chemical and physical stability. The high mobility of oxygen vacancies in CeO_2 with the fluorite structure determined its easy reducibility and high catalytic activity in redox reactions.[175] The presence of the cerium ions in mixed heterometallic oxides $MCeO_{2-x}$ modified the catalytic properties of the overall system as a result of chemical and electronic synergism between highly dispersed components. In addition, the presence of the Ce^{+3} and Ce^{+4} ions favoured the oxygen exchange with the gas phase.[176]

Recently, numerous studies dealing with copper-containing cerium oxide catalysts have been published. This trend is associated with the fact that such systems possess high catalytic activity in reactions of carbon monoxide and methane oxidation,[177–179] SO_2 reduction with carbon monoxide,[180–182] NO reduction,[183, 184] wet oxidation of phenol,[185] as well as the high activity and selectivity in carbon monoxide oxidation in excess hydrogen.[186, 187]

The synthesis of $CuO-CeO_2$ catalysts was carried out by different methods, for example, co-precipitation, sol–gel process, impregnation, combustion, *etc.*[188, 189] The effect of the synthetic method on the physicochemical and catalytic properties of $CuO-CeO_2$ catalysts was studied.[188] The efficiency of catalysts prepared by the co-precipitation, combustion, impregnation and hydrothermal methods was compared for the reaction of selective CO oxidation. It was concluded that the catalyst prepared by the combustion method exhibited the best performance (selectivity and activity). This method produced a mixed oxide in which the highly dispersed copper oxide layer strongly interacted with the ceria surface. The thus synthesized catalysts were resistant to deactivation in the presence of both CO_2 and a mixture of CO_2 and H_2O. Depending on the synthetic method, the catalytic activity of samples was observed to decrease in the following sequence:

combustion method > hydrothermal method ≫

≫ co-precipitation > impregnation.

It should be noted that catalysts synthesized by the first two methods represented bulk mixed oxides whereas the last method produced copper oxides deposited on the surface of pre-formed ceria (support).

The synthesis of $CuO-CeO_2$ catalysts by magnetron sputtering and sol–gel methods was described.[190, 191] The synthesized catalysts possessed high activity and selectivity in CO oxidation due to strong interactions between the highly dispersed CuO clusters and the CeO_2 surface, which resulted in the formation of a solid solution in the Cu–Ce–O system. These catalysts proved to be more active and selective at low reaction temperatures as compared with platinum catalysts conventionally used in this process. As opposed to gold-containing catalyst, they proved to be less active but more selective and heat resistant.[192] Ceria doped with the copper cations also demonstrated excellent catalytic properties in the direct CO-assisted reduction of SO_2 to sulfur [193] and also in low-temperature methane oxidation.[194]

The synthesis of Cu–Ce–O complex oxide systems by the impregnation of pre-formed ceria and by the microemulsion co-precipitation of copper and cerium nitrates is described.[32] The resulting catalysts were characterized by XRD, Raman spectroscopy, high resolution electron microscopy and XPS methods. The synthesized nanostructured samples proved active in the selective CO oxidation in the presence of hydrogen. It was shown that different synthetic methods afforded catalysts with different structures, which manifested in different catalytic properties. Thus a catalysts prepared by the impregnation method represented a copper oxide layer on a ceria support, whereas a catalyst prepared by microemulsion co-precipitation represented a complex oxide in which copper oxide components were distributed over the surface of a Ce–Cu mixed oxide. In the latter case, the stronger interactions of surface CuO grains with the Ce–Cu–O support led to the finer distribution of copper

over the surface and favoured the formation of oxygen vacancies. This was the reason for the enhanced catalytic activity of this catalyst in the reaction of CO oxidation in excess hydrogen.

The $CuO-CeO_2$ catalyst was also prepared [195] by the hydrothermal method under different conditions from an ethanolic solution containing $Ce(NO_3)_3$, $Cu(NO_3)_2$, cetyltrimethylammonium bromide (CTAB) and an excess of NH_4OH followed by ageing and calcination. The effect of synthetic conditions on the catalytic performance in the reaction of CO oxidation in the presence of excess hydrogen was evaluated by the XRD, TPR and temperature-programmed desorption (TPD) of CO methods. By changing the CTAB : Ce ratio and the hydrothermal ageing time (from 0.5 to 6 h) the catalytic activity of the final mixed oxide could be increased. Thus, it became possible to effectively control the dependence 'catalyst phase composition → catalyst activity/selectivity' in the reaction of CO oxidation in excess hydrogen. The $CuO-CeO_2$ catalyst prepared for the optimal CTAB : Ce = 1 : 1 ratio and the hydrothermal ageing time of 1 h demonstrated the best catalytic performance (the CO conversion higher than 99.2% at 120–140 °C, 100% selectivity at temperatures below 110°C). Diffraction patterns of samples with different CTAB : Ce ratios and ageing times have demonstrated that the fluorite structure was typical of all samples. For $0.5 < CTAB : Ce < 1$, no changes were revealed in reflections nor in their intensity. The increase in the CTAB : Ce ratio resulted in less pronounced broadening of reflections and the increase in their intensity, which pointed to the coarsening of grains. The change of the hydrothermal ageing time from 1 to 2 h did not cause any substantial modifications in the diffraction pattern, which suggests that CeO_2 grains were closely packed and the CuO_x particles were in the highly dispersed state on the CeO_2 surface. According to the TPR results, in the studied materials, the nanosized oxide clusters CuO_x that underwent reduction were either chemically bound with the surface or adsorbed on the latter. Insofar as the diffraction patterns contained no reflections of bulk CuO, it can be concluded that the copper oxide clusters uniformly distributed over the surface of bulk ceria were responsible for the catalytic properties of this system.

The analogous data on the structure and phase composition of copper–cerium oxide catalysts was obtained in another study.[196] An optimum composition of a catalyst for selective CO oxidation was claimed. Particularly, it was shown that for small contents ($\leqslant 5$ mass %) of copper incorporated into the CeO_2 lattice, the active components represented disordered copper oxide clusters. The increase in the copper content (> 10 mass %) led to the formation of the CuO bulk phase, which caused catalyst deactivation. As in the former study,[195] the high catalytic activity was associated with the formation of highly dispersed copper(II) oxide clusters and with the copper ions that formed strong bonds with CeO_2.

Copper–cerium oxide catalysts obtained by impregnation of ordered mesoporous zirconium-doped (Si : Zr = 7) silica were tested in CO selective oxidation.[197–199] The properties of this catalyst were compared with those of a catalyst with the same composition but prepared by applying copper and cerium oxide on non-doped silica. Both catalysts demonstrated good performance as regards the activity and selectivity in CO oxidation, especially in the temperature range of 115–140 °C, which made them promising (from the technological viewpoint) for fuel cells. No noticeable difference was observed in the activity of samples with the copper content from 6 mass % to 12 mass %. Further increase in the copper content led to the formation of the CuO bulk phase, which was reduced to metallic copper in the course of the reaction and proved to be inactive in selective oxidation.

To conclude, we consider recent publications,[200, 201] which describe the use of the co-precipitation method for the preparation of mixed oxides based on CeO_2 or $Ce_{1-x}M_xO_{2-\delta}$ (M = Gd, Ho) containing either the Cu and Ni ions or only the Ni ions. Catalysts with the Ce–Ni–O composition exhibited high catalytic activity in the low-temperature oxidative dehydrogenation of propane [200] and the Cu-Ni/CeO_2 and Cu-Ni/$Ce_{1-x}M_xO_2$ catalysts (M = Gd, Ho) proved to be active in direct methane oxidation.

The synthesis of Ce–Ni–O catalysts included co-precipitation of an oxalate gel prepared by mixing ethanolic solutions of metal nitrates with an excess of oxalic acid and subsequent calcination.[200] The catalytic activity of prepared samples was compared with the activities of pure oxides CeO_2 and NiO prepared by the same method and also with the activities of samples prepared by co-precipitation from aqueous solutions and by the conventional impregnation method. The Ce–Ni–O catalyst exhibited the highest catalytic properties in the low-temperature (275 °C) oxidative dehydrogenation of propane (C_3H_8 conversion of 12.8%; selectivity of 82.7% with respect to C_3H_6 and 17.3% with respect to CO_2; the yield of propene 10.6%), which favourably compares it with the vanadium–magnesium oxide catalyst conventionally used in this reaction but operating only at temperatures above 500 °C. Scanning electron microscopic studies have shown that the Ce–Ni–O catalyst had a uniform ($d \approx 14$ μm) doughnut-like macrostructure different from that of samples prepared by other techniques. The uniform NiO dispersion throughout the catalyst volume and the formation of oxygen vacancies due to incorporation of Ni^{2+} ions into the CeO_2 lattice distinguished this sample from the analogous oxide prepared by co-precipitation of oxalates from their aqueous solutions. The latter sample represented a mixture of individual CeO_2 and NiO species. Thus, the excellent catalytic performance of the Ce–Ni–O oxide prepared by co-precipitation of metal oxalates from ethanolic solution were due to the synthetic method that provided the enhanced concentration of active oxygen surface sites and the higher dispersion of the NiO species. Presumably, such a high activity could also be the result of the formation of a unique doughnutlike macrostructure.

The samples of Cu-Ni/CeO_2 and Cu-Ni/$Ce_{1-x}M_xO_{2-\delta}$ (M = Gd, Tb) were prepared by microemulsion co-precipitation.[201] The samples were tested as the candidates for anodes in oxide fuel cells of direct methanol oxidation. The obtained data suggested that the Ni ions and the Gd or Tb dopant ions had a considerable effect on the structure, catalytic and electrophysical properties of these oxide systems. It was shown that the activity of polymetallic oxides in methane oxidation varied in the following order:

$$Cu-Ni/CeGdO > Cu-Ni/CeTbO > Cu-Ni/CeO_2.$$

It was assumed that doping ceria with gadolinium and terbium improved the redox and transport properties of this material, while the formation of a Cu–Ni alloy increased the catalytic activity.

2. Unusual transformations of noble metal nanoclusters applied on the Al_2O_3 surface

Recent TEM and SEM studies of the long-known catalysts containing small amounts of Al_2O_3-supported noble metals ($\leqslant$0.6 mass % Pt or Rh) led to an unexpected result, namely, revealed the interaction of noble metal atoms with γ- and β-Al_2O_3. Thus it was shown [202–204] that nanosized Pt clusters reacted with alumina to form Pt_2Al, $PtAl_2$ and Pt_8Al_{21} intermetallic compounds, which gave rise to nucleation of cationic vacancies on the surface of γ- and β-Al_2O_3. It was reported [205] that the formation of such cationic vacancies during the reductive activation of the industrial alumina–platinum catalyst Pt/Al_2O_3(F) (AP-64) led to radical changes in its selectivity in ethanol conversion. Whereas the partially reduced catalyst exhibited activity in the ethanol steam reforming to syngas, this catalyst subjected to long-term reduction was selective with respect to reductive dehydration of ethanol to alkanes. Presumably, the reason for such changes in the catalytic selectivity was the interaction of the aforementioned cationic vacancies, which exhibited aprotic acidity, with water vapour formed during the reduction, which was followed by the transformation of aprotic sites into strong protic sites responsible for oligomerization.

It was reported [206–208] that the nuclei of highly dispersed platinum oxide species interacted with the support in the initial stage of formation of platinum nanoclusters on an oxide support. Obviously, such unusual transformations could proceed in metastable systems on the alumina surface commonly characterized by the high defect concentration. The ^{27}Al NMR spectroscopic data [209] demonstrated that thermal activation led to the formation of a considerable amount of five-coordinate aluminium ions in addition to four- and eight-coordinate ions on the γ-Al_2O_3 surface. It was shown that the formation of the alumina–platinum catalyst included strong interaction of the platinum ions exclusively with the five-coordinate aluminium ions, which led to saturation of the local coordination environment of the latter ions to octahedral.

It was found [210, 211] that the reductive activation of a catalyst prepared by applying the presynthesized bimetallic palladium–zinc acetate complex on Al_2O_3 afforded Pd–Zn metal clusters. At the same time, the activation of a catalyst prepared by deposition of monometallic acetate complexes $Pd(OAc)_4$ and $Zn(OAc)_2$ onto Al_2O_3 resulted in the formation of oxides of these metals on the support surface. In the latter case, for the small amount of applied components (up to $\sim$1.5 mass %), the catalyst exhibited high activity in the selective hydrogenation of acetylene to ethylene.

Thus, the dependence of the phase composition of catalyst active components on the synthetic methods and the nature of precursors as well as on the possibility of formation of metastable surface phases, which includes the phases involving atoms of stable oxides, made an important contribution to the studies of catalytic systems in which the surface defectiveness of oxide supports determines the non-equilibrium phase transformations.

V. Nanosized iron-containing complex oxide catalysts synthesized by the alkoxy method

1. Iron–aluminium oxide catalysts in the liquid-phase oxidation of hexadecane, cumene and isopentyl alcohol

The high activity in liquid-phase oxidation of hydrocarbons is also typical of mixed iron–aluminium oxide catalysts Fe–Al–O prepared by the alkoxy method from aluminium isopropoxide and iron acetylacetonate.[212–216] The evolution of the phase composition of these catalysts in all steps of their formation was followed by the EXAFS, Mössbauer spectroscopy, EPR and magnetic susceptibility methods. The obtained results served as the basis for gaining insight into the relationship between the catalyst structure and the catalytic activity in the liquid-phase oxidation of cumene, hexadecane and isopentyl alcohol.

Iron–aluminium oxide catalysts prepared by the alkoxy method remained X-ray amorphous in all steps of their formation, from the gel to the oxide. According to the magnetic susceptibility data, these systems were antiferromagnetic and contained high-spin Fe^{3+} ions, which suggested that the sol–gel reaction produced Fe–O–Fe structural elements in which iron ions were bound by superexchange interactions of the antiferromagnetic type. These results were confirmed by EXAFS data (Table 1). The magnetic behaviour of all samples was typical of an ensemble of superparamagnetic oxide clusters with the ferrimagnetic type of ordering.

Table 1. Structure of Fe^{3+} complexes in the Fe–Al–O systems according to EXAFS data.

Fe–Al–O	CN	Bond type	R/Å
Gel	6.2 ± 0.8	Fe–O	1.96
		Fe–Fe	3.00
		Fe–Fe	3.62
		Fe–Fe	4.08
		Fe–Fe	4.45
Oxide (2.5 mass % Fe)	5.4 ± 0.8	Fe–O	1.96
		Fe–Fe	2.60
		Fe–Fe	2.84
		Fe–Fe	3.10
		Fe–Fe	2.84
		Fe–Fe	4.40

A comparison of interatomic distances in the synthesized gels with the distances known for the pseudoboehmite and amorphous aluminium hydroxide structures made it possible to assume that the structure of crystallographically amorphous gels corresponds to that of local octahedra with the empirical formula $[Al(OH)_6]$ in which the Al^{3+} ions are isomorphically substituted by the Fe^{3+} ions.[215] However, the absence of Fe–Fe(Al) distances with R = 3.5 and 4.5 Å suggested that the iron ions form a thin film on γ-Al_2O_3 faces rather than are distributed in the bulk. Upon thermal treatment, microheterogenization of the gel matrix occurred, which was accompanied by the formation of both individual iron ions and ferromagnetic iron oxide clusters with superparamagnetic properties. The latter apparently formed as a result of elongation of the Fe–O–Fe fragments. The general trend traced for iron-aluminium oxide samples was that the number of magnetic

Table 2. The main kinetic parameters (maximum rate W_{max} and autoacceleration factor φ) for the reaction of hexadecane oxidation in the presence of mixed iron–aluminium oxide catalysts (samples **2**–**5**) and catalytic systems γ-Al_2O_3 (**1**), γ-Fe_2O_3 + 10 mass % Al_2O_3 (**6**), γ-Fe_2O_3 (**7**).

Sample	Catalyst	Iron content (mass %)	Specific surface / $m^2\ g^{-1}$	$W_{max} \times 10^4$ / mol litre^{-1} s^{-1}	φ / mol (litre m^2 g s)$^{-1}$
1	γ-Al_2O_3	0	305	3.3	0.180
2	$Fe_xAl_{2-x}O_3$	2.5	296	6.0	0.220
3	$Fe_xAl_{2-x}O_3$	6.2	290	8.4	0.250
4	$Fe_xAl_{2-x}O_3$	13.6	290	11.2	0.310
5	$Fe_xAl_{2-x}O_3$	20.0	285	13.0	0.430
6	γ-Fe_2O_3 + 10 mass % Al_2O_3	63.0	140	4.8	0.225
7	γ-Fe_2O_3	70.0	190	8.9	0.270

Note. In the absence of catalyst, $W_{max} = 4.7 \times 10^4$ mol litre^{-1} s^{-1} and $\varphi = 0.220$ mol (litre m^2 g s)$^{-1}$.

γ-Fe_2O_3 clusters progressively increased with the increase in the concentration of incorporated iron. An indirect confirmation of this model was the data on the specific surface of iron–aluminium oxides (Table 2, samples **2**–**5**), where the latter remained virtually unchanged with the variation in the amount of incorporated iron.[213]

The data from Mössbauer spectroscopy and magnetic measurements showed that γ-Fe_2O_3 clusters in Fe—Al—O samples containing $\leqslant$10 mass % Fe measured $\sim$3–5 nm. For metal oxides with the higher iron content, the size of the oxide phase Fe_xO_y nuclei increased to $\langle d \rangle \approx 8$–10 nm. A γ-$Fe_2O_3$ sample represented an ensemble of superparamagnetic oxide particles ($\langle d \rangle \approx 8$ nm) with the clearly pronounced magnetic non-uniformity and a defective structure. This results in the formation of structural and electronic heterogeneities (defects), which probably favoured the initiation of the process of liquid-phase oxidation of substrates.[217]

Mixed iron–aluminium oxide catalysts with different iron content synthesized by the alkoxy method were tested in reactions of liquid-phase oxidation of hexadecane (see Table 2), cumene (Table 3) and isopentyl alcohol.[212–216] The catalytic performance of samples **2**–**5** was compared with that of sample **6**, prepared by co-precipitation of iron and aluminium hydroxides from aqueous solutions of inorganic salts.

Table 3. Catalytic activity of iron–aluminium oxide catalysts prepared by the alkoxy method in the liquid-phase cumene oxidation.

Catalyst	Fe content (mass %)	$W_0 \times 10^5$ (see [a])	$W_{max} \times 10^5$ (see [a])	φ (see [b])
γ-Fe_2O_3	70.0	1.20 ± 0.03	1.62 ± 0.03	0.90 ± 0.04
$Fe_xAl_{2-x}O_3$	1.0	0.40 ± 0.03	1.61 ± 0.03	1.80 ± 0.05
	2.5	0.81 ± 0.03	3.72 ± 0.03	3.62 ± 0.05
	6.2	1.14 ± 0.03	3.90 ± 0.04	4.22 ± 0.04
	13.6	1.12 ± 0.03	3.63 ± 0.04	3.91 ± 0.04

[a] In mol litre^{-1} s^{-1}; [b] in mol (litre m^2 g s)$^{-1}$.

Iron–aluminium oxide catalysts tested in hexadecane oxidation were synthesized by calcination of the corresponding gels with stepwise temperature increase to 500 °C in 4 h.

Each of iron-containing oxides (samples **2**–**7**), except for catalyst **6**, promoted oxidation, whereas γ-Al_2O_3 (sample **1**) inhibited this process. For samples **2**–**5** prepared by the alkoxy method, the maximum steady-state oxidation rate and the autoaccelaration factor were shown to increase with the increase in the iron content to reach the maximum values at 20 mass %. Dilution of γ-Fe_2O_3 with alumina (sample **6**) resulted in the loss of catalytic activity. In the series of iron-containing samples, sample **6** can be taken as the reference because its catalytic activity is negligible and the kinetic parameters of reactions in its presence are comparable with parameters of reactions without catalysts.

Table 3 shows the kinetic parameters of cumene oxidation in the presence of iron–aluminium oxide catalysts synthesized by the alkoxy method and in the presence of γ-Fe_2O_3. It should be noted that in the absence of catalysts virtually no oxygen absorption was observed.

As follows from Table 3, the rate of cumene oxidation (T = 90 °C) increased with the increase in the iron content in the sample from 1.0 mass % to 6.2 mass %; however, with further increase in the iron concentration, the rate decreased insignificantly. Analogous data were obtained for hexane and isopentyl alcohol oxidation.[212] The analysis of kinetic parameters has shown that the initiation of substrate oxidation occurred on the surface of active components the size of which affected the oxygen absorption rate.[216, 217]

The inclusion of a small amount of aluminium into the γ-Fe_2O_3 lattice did not change the lattice pattern and the size of microparticles. However, the incoporation of non-magnetic aluminium ions in the chain of Fe—O—Fe superexchange interactions decreases the effective magnetic moments of sublattices and the values of exchange integrals and increases the scatter of interatomic distances. This was accompanied by changes in the nature of electronic defects, which apparently affected the kinetic parameters of the oxidation process.

Assessment of the relative amount of iron magnetic clusters distributed over the surface of catalytic systems was carried out based on the data from Mössbauer spectroscopy. It was shown that the increase in the relative amount of these clusters favoured the proportional increase in the hexadiene and cumene oxidation rates.[215, 216]

Studying the electronic structure of magnetoactive iron oxides[217] showed that the surface of clusters of non-stoichiometric γ-Fe_2O_3 in the cationic and anionic positions was enriched in crystallographic defects such as cationic vacancies around which terminal oxygen bonds concentrated, which could easily be transformed into active radical anions by thermal excitation.[217, 218] The formation of the ferryl radical anions on the oxide surface as well as the formation of the vanadyl, chromyl and molybdyl[219] surface groups was accompanied by the shift of the electron density in the Fe—O bond to the metal atom and the increase in the

interatomic distance. It is high reactivity of the radical anions formed upon thermal excitation of the oxygen atoms that was assumed to be the reason for the enhanced catalytic activity of highly dispersed clusters of non-stoichiometric γ-Fe_2O_3.

The obtained results suggest that the mechanism of formation and the structure of iron–aluminium oxides depend on the synthetic method. Thus in the co-precipitation of iron and aluminium hydroxides from aqueous solutions of inorganic salts (see Table 2, sample **6**), doping of the γ-Fe_2O_3 lattice with the aluminium ions proceeded mainly on the surface of particles. This led to spinel iron–aluminium oxide and simultaneously decreased the specific surface of samples as compared with catalysts synthesized by the alkoxy method from organic metal complexes. The presence of structural heterogeneity was confirmed by magnetic data according to which the samples contained two magnetic phases, namely, iron–aluminium spinel and γ-Fe_2O_3 phases.

Thus, for Fe–Al–O samples prepared by the alkoxy method, an increase in the iron concentration led to an increase in the number of active sites that apparently represented the oxygen ions of superparamagnetic γ-Fe_2O_3 clusters, which can be thermally activated. Upon insignificant increase in the size of γ-Fe_2O_3 surface clusters and increase in their concentration, the number of active sites increased, which was manifested by the increase in the oxidation rates of hexadecane and cumene in parallel with the increase in the concentration of iron incorporated into alumina (Fig. 1).

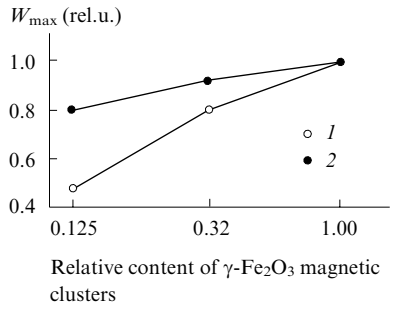


Figure 1. Dependences of the reaction rate of liquid-phase oxidation of hexadecane (*1*) and cumene (*2*) on the number of γ-Fe_2O_3 magnetic clusters in catalysts synthesized by the alkoxy method.

2. Iron–aluminium oxide catalysts in CO hydrogenation reaction

Iron–aluminium oxides exhibited high selectivity not only in oxidation reactions, but also in CO hydrogenation. The results of detailed studies of structure–catalytic activity relationships of iron–aluminium oxides in the latter reaction were published.[220,221] Structural studies were carried out by *in situ* static magnetic susceptibility and Mössbauer spectroscopic measurements.

The aforementioned publications[220,221] dealt with iron–aluminium oxides with different iron content and also with zirconium-doped iron–aluminium oxide (Table 4). All samples were prepared by the alkoxy method in the same way as for iron–aluminium oxides described in Section V.1 followed by thermal treatment in atmosphere of different gases (hydrogen or air). According to XRD data, all iron-containing catalysts tested in CO hydrogenation were crystallographically amorphous.

As follows from Table 4, the increase in the iron content to 8 mass % (sample **C**) enhanced both the overall activity and the degree of CO conversion to alkylaromatic hydrocarbons. It should be noted that catalysts **A**–**C** possess high selectivity in the formation of alkylbenzenes AlkPh (Alk = C_1–C_8), the mode of preactivation strongly affecting the catalytic properties of the catalyst. In contrast to one-step treatment (H_2), the two-step treatment (O_2, H_2) of samples **A**–**C** led to a decrease in their overall activity and selectivity with respect to the formation of lower alkylbenzenes (Alk = C_1–C_3) with the simultaneous increase in selectivity with respect to formation of higher alkylbenzenes

Table 4. The overall activity and the yield of reaction products for CO hydrogenation in the presence of iron–aluminium oxide catalysts prepared by the alkoxy method.

Catalyst	Iron content (mass %)	Activation	W (see [a])	Liquid products (%)				Gaseous products (%)	
				AlkPh		alkenes	alkanes	C_1–C_5	CO_2
				C_1–C_3-Ph	C_4–C_8-Ph				
A	2.5	(H_2)	0.6	48.3	trace	trace	trace	2.5	49.2
		(O_2, H_2)	0.4	27.3	6.2	trace	trace	2.0	64.0
B	5.6	(H_2)	1.8	46.0	trace	trace	trace	3.0	51.0
		(O_2, H_2)	1.1	30.0	8.0	trace	trace	3.5	58.5
C	8.0	(H_2)	3.5	48.0	trace	trace	trace	3.2	48.8
		(O_2, H_2)	1.6	30.0	11.8	trace	trace	3.5	54.7
C–Zr (Zr = 0.4 mass %)	8.0	(O_2, H_2)	0.7	52.0	trace	trace	trace	3.0	45.0
D	15.0	(H_2)	2.5	trace	2.0	6.0	20.0	8.0	64.0
		(O_2, H_2)	1.7	trace	trace	3.0	22.0	10.0	65.0
E	20.0	(H_2)	1.4	trace	trace	5.0	21.0	8.4	65.6
		(O_2, H_2)	1.1	trace	trace	2.0	20.0	11.0	67.0

Note. Designations: (H_2) is activation of gels by hydrogen treatment at 400 °C, 1 atm, 4 h; (O_2, H_2) is activation of gels by two-step consecutive treatment in air at 500 °C, 1 atm, 4 h and in hydrogen at 400 °C, 1 atm, 4 h.[221] [a] W is the rate of CO conversion in μmol litre^{-1} min^{-1}.

(Alk = C_4-C_8). The higher selectivity with respect to lower alkylbenzenes (Alk = C_1-C_3) was exhibited by zirconium-modified catalyst **C−Zr**. Catalyst **E** proved to be non-selective in CO reduction to alkylaromatic hydrocarbons irrespective of the preactivation method.

With further increase in the iron content in the catalyst (>8 mass %), the selectivity of the process dramatically decreased. Insofar as all catalysts had virtually the same specific surfaces (S_{sp} = 380–400 $m^2\ g^{-1}$), it is evident that the catalytic properties depended on the nature of iron-containing sites. As follows from the results shown, the synthesis of alkylaromatic hydrocarbons from CO and H_2 is characterized by higher structural sensitivity than the liquid-phase oxidation.

The data from Mössbauer spectroscopy show that the gel preactivation has a considerable effect on the structure of catalysts. Thus samples **A–C** subjected to one-step activation (H_2) contained high-spin Fe^{2+} ions and Fe^{3+} ions in the amorphous aluminium oxide matrix. No α-Fe clusters were found in samples **A–C** subjected to one-step activation even in the case of their enrichment in ^{57}Fe. In contrast, the two-step activation (O_2, H_2) of samples **A–C** led to the formation of metallic iron in addition to paramagnetic Fe^{2+} and Fe^{3+} oxides.

The highest activity in the synthesis of alkylaromatic hydrocarbons from CO and H_2 was exhibited by catalyst **C** subjected to one-step activation.[220] Mössbauer spectroscopic studies have shown that this catalyst consisted of a mixture of iron carbide (magnetically ordered χ-Fe_2C_5 clusters measuring 3 ± 0.5 nm in average) and an iron-substituted γ-$Fe_xAl_{2-x}O_3$ spinel.

After its pretreatment with hydrogen, the structure of catalyst **E** with the highest iron content substantially differed from the structures of catalysts **A−D**. After the reduction, almost the whole sample **E** transformed to a mixture of α-Fe (~46%) and γ-$Fe_xAl_{2-x}O_3$ with high-spin Fe^{3+} (~29%) and Fe^{2+} (~25%) ions. However, low-temperature Mössbauer measurements indicated that small ferrimagnetic spinel clusters were present in sample **E**. As a result, this catalyst turned out to have the highest degree of reduction, which correlated with virtually complete loss of its selectivity in alkylaromatic hydrocarbon synthesis.

A comparison of the degree of reduction of catalysts **C** after their one- or two-step activation shows that their selectivities in alkylbenzene synthesis are the higher the lower the degree of their reduction. This is probably associated with the fact that after the treatment with oxygen, a part of original gel **C** transformed into nanoclusters with the magnetite structure.

After the CO hydrogenation reaction, catalyst **E** proved to be in the highest reduction state. It was found that the relative content of metallic iron (α-Fe) in this sample reached ~87%.

The result of two-step activation of catalyst **C–Zr** was similar to that of one-step activation of catalysts **A−C**. From the analysis of structural peculiarities of the most selective catalyst **C–Zr** it was suggested that its modification with zirconium has a dual effect. First, the substitution of the zirconium ions for the aluminium atoms results in violation of the local symmetry of cationic positions in the structure and changes in the Mössbauer parameters of the Fe^{3+} ions. Second, Zr inhibits the mobility of lattice oxygen thus slowing down the formation of magnetic clusters and, the more so, their aggregation.

According to the data from Mössbauer spectroscopy, the zirconium-doped catalyst comprised small iron oxide clusters with $\langle d \rangle \approx 3-7$ nm, the γ-$Fe_xZr_yAl_{2-x-y}O_3$ matrix with discrete Fe^{3+} and Fe^{2+} ions and a new magnetic structure (its relative content did not exceed 3%–5%). The latter structure with spectral parameters close to those of iron carbide Fe_xC can be defined as intermediate between ferrite (tetragonal martensite) and carbide $Fe_{2-x}C$ structures. The role of oxygen vacancies in the hydrocarbon chain growth was also analyzed.[220]

It was concluded that stabilization of the structure of iron–aluminium oxide with zirconium ions allowed the iron-containing particles to retain their uniform highly disperse state in the course of catalyst evolution, *i.e.*, the state favourable for the enhanced selectivity of such a catalyst with respect to formation of lower alkylbenzenes from CO and H_2.

3. The process of formation of $Fe_xM_{1-0.75x}O_{2\pm\delta}$ ($M = Zr^{4+}$, Ti^{4+}) binary oxides from gels prepared by the alkoxy synthesis

Interesting results were obtained[35] when studying the formation of binary iron-containing oxides with the general composition $Fe_xM_{1-0.75x}O_{2\pm\delta}$ ($M = Zr^{4+}$, Ti^{4+}) from the corresponding gels synthesized by the alkoxy method. According to the data from elemental analysis, IR-spectroscopy and magnetic susceptibility measurements, the crystallographically amorphous gels synthesized from iron(III) acetylacetonate and tetra(isobutoxy)titanium or tetra(isopropoxy)zirconium contained organic fragments of the original complexes and the metal ions. Heat treatment of these gels at 500 °C for 6 h led to the loss of organic fragments and crystallization. According to XRD analysis, this resulted in the formation of solid solutions of isomorphous substitution with the empirical composition $Fe_xZr(Ti)_{1-0.75x}O_{2\pm\delta}$ ($0.01 < x < 0.17$ in the Fe−Zr−O system and $0.01 < x < 0.14$ in the Fe−Ti−O system).

Extended X-ray absorption fine structure studies of the iron–zirconium oxide gel revealed the formation of small clusters with the structure close to that of ZrO_2, which were linked to one another by organic fragments or by iron ions in the octahedral environment. For the Fe-ZrO_2 gel, the following three main interatomic distances were found: R = 1.94 Å (Fe−O), R = 3.12 Å (Fe−Fe) and R = 3.30 Å (Fe−Zr). The sample formed after crystallization contained, in addition to these iron-involving bonds, two other interatomic distances R = 2.14 and 3.61 Å, which were attributed to the Zr−O and Zr−Zr bonds, respectively. An insignificant change in interatomic distances involving Fe atoms upon crystallization of the iron–zirconium oxide sample suggested that the formation of the iron oxide structure started already in the gel and that the crystallization involved only the removal of the organic fragments, which favoured the contraction of cubic ZrO_2 polyhedra formed in the gel. As a result, the cubic metal oxide ZrO_2 with slight structural deviations formed on the faces of which the epitaxial Fe_2O_3 film grew. Due to the great difference in the Zr−O and Fe−O distances, no more than one Fe^{3+} layer could exist on the ZrO_2 face. Therefore, the observed Fe−Fe distance of 3.13 Å apparently pertained to the iron ions belonging to different ZrO_2 clusters.

Thus, the structure of the iron–zirconium oxide catalyst represents flattened cubic clusters of zirconium oxide with $\langle d \rangle \approx 10-12$ nm on the faces of which epitaxial films of iron oxide formed.

The formation of the $Fe_xTi_{1-0.75x}O_{2\pm\delta}$ complex oxide structure also began in the course of the alkoxy synthesis and proceeded in the analogous manner as the $Fe_xZr_{1-0.75x}O_{2\pm\delta}$ formation.[7] In the Fe–Ti–O system, in the same manner as in its zirconate analogue, the iron ions did not incorporate into the TiO_2 structure but were stabilized on the (110) plane incompletely occupied with the iron ions. Thus, the nanostructured materials synthesized by the alkoxy method represent highly dispersed particles of titanium or zirconium oxides stabilized by the iron ions.[35] This stabilization determines the low catalytic activity and the high selectivity of these systems in the synthesis of gaseous alkenes C_2-C_5 and liquid aromatic compounds from CO and H_2.

Insofar as titanium dioxide was a part of the $Fe_xTi_{1-0.75x}O_{2\pm\delta}$ sample, it seemed natural to assume that this mixed oxide was catalytically active in photoreactions. The catalytic activity of colloidal solutions of nanostructured iron–titanium oxide catalysts synthesized by the alkoxy method from tetra(isopropoxy)titanium and iron(III) acetylacetonate in photooxidation of methanol was assessed.[222] A comparison was made of the structures and the catalytic activities of TiO_2 with and without iron-dopant prepared by the alkoxy method from inorganic or organic precursors.

The results of studies by HRTEM and cryo-TEM methods have shown that all titanium-containing photocatalysts studied possessed the same particle size (2–3 nm) and the same structure (anatase) irrespective of the type of the starting reagents. It was stated[222] that the iron ions are incorporated into the TiO_2 lattice though no clear evidence was provided; this is in contrast to our previous studies[35] where a conclusion was made that the iron ions form a film on the TiO_2 faces without being incorporated into the titania lattice. Despite the observed structural similarity of studied titanium-containing samples prepared from inorganic and organic precursors, they exhibited different photocatalytic activities. The highest photocatalytic activity was exhibited by an iron–titanate catalyst synthesized from organic precursors (the quantum yield of formaldehyde formation was used as the photocatalytic characteristic). This was associated with the formation of a supramolecular structure in this material, namely, chain-like aggregates. As a result of the formation of such a structure, the energy transfer from one particle to another is possible, which makes the substrate molecules adsorbed in any site of this colloidal aggregate accessible for the photocatalysis (the 'antenna' effect). Thus, it was demonstrated that nanostructured iron–titanium oxide catalysts synthesized by the alkoxy method from organic precursors could serve as shallow charge traps.

VI. The effect of the size factor on the catalytic properties of iron oxide catalysts on porous supports

1. Iron oxide nanoparticles on porous TiO_2

The analysis of several publications[223–226] on the synthesis and catalytic properties of iron oxide samples synthesized by sonication made it possible to reveal the relationship between the catalytic activity in cyclohexane oxidation and the catalyst size characteristics.

The results of cyclohexane oxidation in the presence of nanostructured crystallographically amorphous oxides FeO/TiO_2 synthesized by iron oxide precipitation from an iron pentacarbonyl solution in decalin onto the surface of commercial titania (Degussa P25) by sonication in air are described.[223] The structures and the particle sizes of synthesized catalysts were established by the XRD and TEM methods. It was shown that the size of spherical FeO/TiO_2 particles was 40 nm. The latter represented titania covered with highly dispersed iron oxide nanoparticles measuring 5–10 nm. The use of this catalyst in cyclohexane oxidation with oxygen (1 atm, 70 °C) afforded a mixture of cyclohexanol and cyclohexanone in the ratio of 1.5 : 1 (conversion 16.5%, selectivity 90%).

This reaction carried out in the presence of highly dispersed iron oxide ($\langle d \rangle \approx 8-10$ nm) also prepared by the sonication[224,226] revealed its lower catalytic activity (conversion 11%) but higher selectivity (up to 95%). The cyclohexanol : cyclohexanone ratio was 2.3 : 1.

Cyclohexane oxidation in the presence of iron oxide supported onto mesoporous titania presynthesized by the sol–gel method from tetra(isopropoxy)titanium proceeded under mild conditions (O_2, 1 atm, 70 °C).[225] This catalyst with the specific surface of 570 $m^2\ g^{-1}$, the average pore size of 1.3 nm and the volume of pores of 0.23 $cm^3\ g^{-1}$ demonstrated the highest activity (cyclohexane conversion was 26%) among the highly dispersed iron oxide samples described above.

Thus, it can be concluded that the use of nanostructured supported iron oxides as the catalysts was more efficient as compared with non-supported iron oxide.

2. Supported superparamagnetic γ-Fe_2O_3 nanoclusters on silica matrices

Stabilization of γ-Fe_2O_3 clusters in a layered silica matrix made these systems efficient catalysts in transformations of chloro alkenes[227] and selective oxidation of hydrogen sulfide contained in natural gas to sulfur.[228] The activity of these catalysts was much higher than that of other supported γ-iron oxide catalysts.[229] It was found that the size factor determined by the nature of the support and the electronic state of γ-Fe_2O_3 nanoclusters had a substantial effect on the catalytic performance of these heterogeneous systems.

Macroscopic magnetization in the temperature range from 2 to 300 K and Mössbauer spectroscopy at 300 K were used to study supported γ-Fe_2O_3 nanoclusters on an activated silica gel matrix (ASGM, specific surface after activation 340 $m^2\ g^{-1}$)[230] and a silica matrix (ASM, specific surface after activation 350 $m^2\ g^{-1}$)[227] prepared by acidic etching of either KCK-2 silica gel with the globular structure (in the former case) or natural vermiculite (in the latter case). The samples were prepared by impregnating ASM or ASGM with a toluene solution of iron(III) acetylacetonate followed by drying in air, evacuation and calcination at 550 °C. All the samples, namely, 2.5 Fe/ASGM, 2.5 Fe/ASM, 4.5 Fe/ASM, 18 Fe/ASM (the percentage of iron in the sample is indicated), were crystallographically amorphous.

The catalysts 2.5 Fe/ASM and 2.5 Fe/ASGM proved to be magnetically heterogeneous and contain two different magnetic phases each. A complex structural study has shown that these phases are represented by magnetically ordered nanosized clusters and paramagnetic iron ions incorporated into the silica lattice. The difference in magnetic properties of 2.5 Fe/ASGM and 2.5 Fe/ASM samples is due to the fact that, in the former, coarse superparamagnetic iron clusters with the antiferromagnetic sublattices

formed on the silica gel surface. A substantial contribution to magnetic properties was made by paramagnetic iron ions that formed complexes with the oxygen ions of silica matrices. The ASM-supported iron oxide clusters had narrower size distribution as compared with clusters on ASGM.

The presence of small magnetic γ-Fe_2O_3 clusters in 2.5 Fe/ASM and 2.5 Fe/ASGM samples was confirmed by the data from their direct and reverse magnetization at $T = 2$ K.[231] Figure 2 shows the hysteresis curves typical of a magnetically ordered material, particularly superparamagnetic γ-Fe_2O_3 clusters with the size $\langle d \rangle \approx 2-3$ nm. After the reaction, the field dependence of magnetization at 2 K was linear (the line *ab* passes through the origin). The analysis of Mössbauer spectra and magnetic properties of samples made it possible to assume that in the course of the catalytic reaction the Fe^{3+} ions in γ-Fe_2O_3 nanoclusters were partly reduced by the chloro alkene to Fe^{2+} ions within a complex in which both the chlorine ions and the oxygen ions of the silica matrix served as the ligands. Probably, this was the reason for the high catalytic activity of γ-Fe_2O_3 nanoparticles.

According to the data from Mössbauer spectroscopy, as the iron content in ASM increased to 4.5 mass % and 18.0 mass %, coarse γ-Fe_2O_3 clusters with the size assessed by magnetization measurements as 6–8 nm formed in the layer silica matrix in addition to small γ-Fe_2O_3 clusters ($\langle d \rangle \approx 2-3$ nm). In this case, with the increase in the iron content, the relative ratio of coarser clusters increased from 0.34 (4.5 Fe/ASM) to 0.50 (18 Fe/ASM).[231]

Iron clusters in the silica matrix differed in size, while their magnetic properties reflected the total contribution made by both these particles and aggregate systems involving them.

The highest catalytic activity was exhibited by the ASM sample with 2.5 mass % of Fe in which Fe^{3+} and Fe^{2+} were present in their paramagnetic state. The catalyst s activity increased with the appearance of magnetically ordered γ-Fe_2O_3 clusters formed as the iron content in the catalyst increased to 15 mass %.

Iron-containing systems on ASM exhibited high activity in selective oxidation of hydrogen sulfide contained in natural gas to sulfur.[228]

$$H_2S + \frac{1}{2}O_2 \longrightarrow S + H_2O.$$

This reaction plays an important role in cleaning gases from toxic hydrogen sulfide by the Claus process, it pertains to the so-called adsorption-catalytic reactions. This means that sulfur formed is deposited in the catalyst pores as the result of which the coarse iron clusters on the surface of different supports are quickly converted to stable and inactive iron sulfides with the loss of catalytic activity.[232]

$$Fe_2O_3 \xrightarrow{S} Fe_{1-x}O_3 \xrightarrow{S} FeS_2.$$

The strong interaction of the iron ions with the ASM support made it possible to longer retain the activity of nanocluster γ-Fe_2O_3/ASM catalysts. It was found that in the presence of this system, the quantitative transformation of hydrogen sulfide to sulfur occurred even at room temperature.[233]

Figure 3 shows the dependence of the extent of hydrogen sulfide conversion on the volume of passed gas in the presence of 2.5 Fe/ASM catalyst, which included the regeneration stage. As is seen, after passage of 13 600 cm^3 of gas containing 0.5 vol.% H_2S, the catalyst activity decreased due to the deposition of elemental sulfur on its surface. After the regeneration stage (melting sulfur out of the surface), the catalyst recovered its activity, which enabled virtually quantitative conversion of hydrogen sulfide.

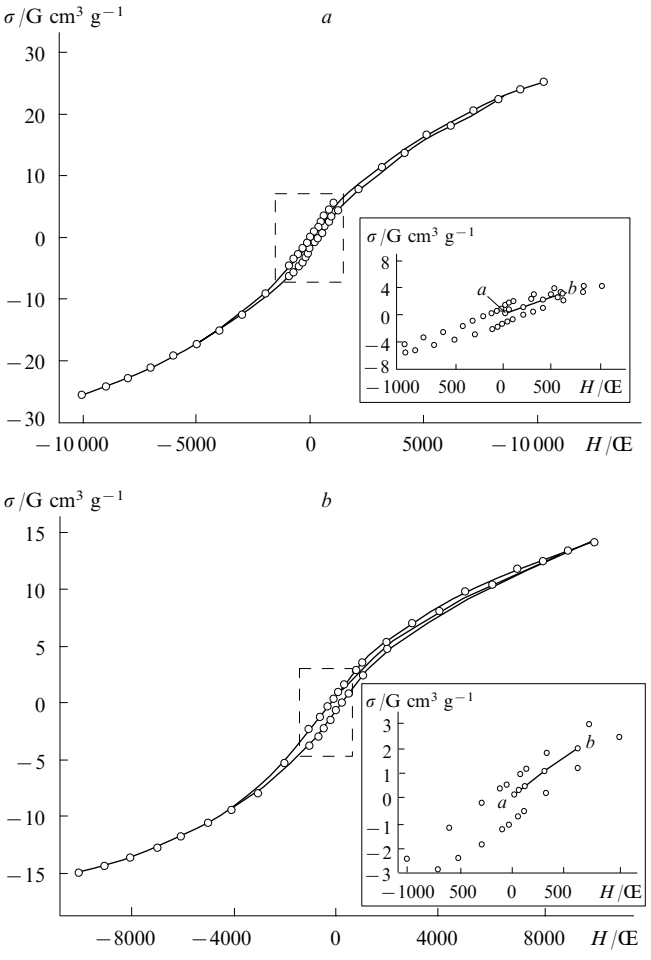


Figure 2. Isotherms of magnetization σ (per g of Fe) at $T = 2$ K for 2.5 Fe/ASM (*a*) and 2.5 Fe/ASGM (*b*) samples.
The inserts show the magnified parts of the hysteresis curve.

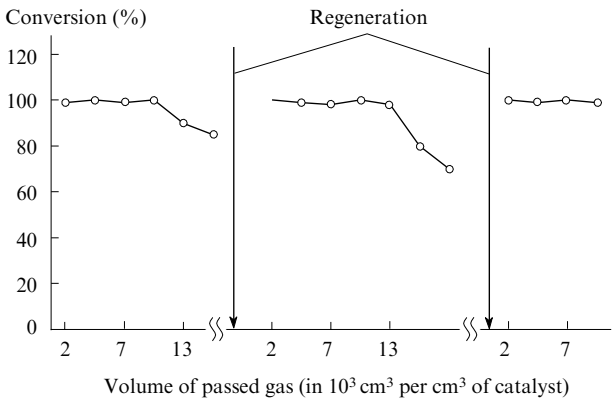


Figure 3. Dependence of the degree of conversion of hydrogen sulfide on the volume of passed gas in the presence of 2.5 Fe/ASM catalyst. The arrows point to the regeneration stages of the latter. Gas composition (vol.%): 0.5 H_2S, 1.25 air, balance CH_4. $T = 25-35$ °C.

At 150–170 °C and the feed flow rate of the hydrogen sulfide-containing gas of up to 5000 h^{-1}, the catalyst activity retained for a long time and the residual hydrogen sulfide content in the gas at the reactor outlet did not exceed 2–5 ppb.[233, 234] The data obtained on studying the catalyst activity and structural evolution during the catalytic process allowed the mechanism of catalysis to be proposed. According to this mechanism, the exchange reactions between the sulfur ions and the oxygen atoms involved the terminal oxygen atoms of non-stoichiometric oxide γ-Fe_2O_3 stabilized by the ASM matrix and were followed by a stage of elemental sulfur deposition on the catalyst surface. The catalytic site regeneration occurred through the addition of oxygen molecules, which was introduced in small amount into the reaction zone, to the reduced iron ions.[227, 235]

3. Iron-containing oxide catalysts in the hydrogenation reaction of brown coal organic mass (COM)

a. A model of the interaction of the iron ions with the COM surface

The processes of hydrogenation of the coal organic mass to hydrocarbons is a strategic direction in the field of non-petroleum fuel production, which is explained by much richer natural coal resources as compared with oil and gas-condensate. The moderate interest in this problem, though, in other alternative approaches as well, was mainly associated with the accessibility of oil. However, the trend to depletion of oil and gas fields determines the necessity of solving this problem. The development of methods of coal organic mass processing has its own rich history.[236–238] The use of principles of the formation of nanosized catalytic systems directly on the surface of coal that is processed and studies on the genesis of active components in the hydrogenation reaction of brown coal organic mass emerged as a new promising approach to solve this problem. It should be noted that the literature contains insufficient information on the structure and evolution of catalytic systems used in this field.

The ability of iron ions to form nanosized non-stoichiometric oxide clusters on the support surface that are stable at high temperatures and elevated pressures makes it possible to prepare efficient heterogeneous systems with highly developed specific surfaces. We used this important property for designing a catalyst for COM hydrogenation. Studies by precision magnetic methods allowed us to follow the changes in the coordination environment of the iron ions on the COM surface in the course of formation of oxide nanoclusters and their subsequent phase transformations. It seemed natural to assume that the activity of the catalysts employed depends to a large extent on the nature of the starting iron complexes used for immobilization on the active coal surface as well as on the structure of iron-containing sites emerged during hydrogenation. In connection with this, we studied the interaction of iron acetylacetonate mono- and bimetallic complexes used as precursors with the brown coal surface.[239, 240]

A monometallic iron-oxide catalyst was prepared by thermolysis of iron(III) acetylacetonate supported onto the coal surface from an aromatic solvent. It was found that chemisorption of iron acetylacetonate occurred on the interface between the organic mass and inorganic inclusions in coal and led to partial decomposition of the original complex.[239, 240] During hydrogenation, the iron-containing component was preferentially obtained in the form of spinel non-stoichiometric oxide particles where the non-stoichiometry factor varied from $x\,FeO \cdot y\,Fe_2O_3$ to γ-Fe_2O_3.

Based on the data from the static magnetic susceptibility measuremens and Mössbauer spectroscopy, the following model was proposed for the interaction of the iron ions with the COM surface. Iron acetylacetonate was adsorbed in defective disordered regions in the coal bulk and decomposed on its interface with inorganic inclusions (α-quartz, silica, iron and aluminium oxides, calcite). In the course of hydrogenation, hydrogen reacted first of all with carbon located in the mentioned quasiamorphous matrix regions, which led to the Fe–C bond cleavage. As COM transformed into hydrocarbons, the iron oxide compounds deposited on the surface of the inactive carbon mass. Simultaneously, they were reduced, recrystallized and formed clusters with the reverse spinel structure of the magnetite type.[239] Experimental data also pointed to the formation of iron metal clusters that were later oxidized with oxygen contained in coal and thus passed to the stable state of superparamagnetic oxide particles. As a result of coal hydrogenation, iron was accumulated in the solid deposit to form massive blocks of a non-stoichiometric magnetite.

b. Phase transformations of nanosized mono- and binuclear iron–cobalt containing catalysts on the COM surface

In continuation of the search for efficient catalysts for hydrogenation of the coal organic mass, we studied the catalytic properties and structural peculiarities of iron-cobalt catalysts prepared from mono- and heteronuclear metal acetylacetonates.[241]

Heteronuclear iron–cobalt acetylacetonate was synthesized by the anodic electrochemical dissolution of an iron–cobalt alloy in acetylacetone. The metal-containing complexes were applied onto the surface of dried coal from an aromatic solvent. The total amount of deposited metals did not exceed 1.5 mass %. Tetralin and a bituminous oil fraction that boiled above 350 °C were used as the liquid-phase hydrogen donors. The catalyst structure was studied by Mössbauer spectroscopy and X-ray diffraction methods.

According to Table 5, after the reduction, the bimetallic catalysts and the iron-containing catalyst provided sufficiently high COM conversion and yield of liquid products.

According to the data from Mössbauer spectroscopy, after the experiment, in sample **2**, two structural types were revealed, namely, a structure intermediate between Fe_3O_4 and γ-Fe_2O_3, which corresponded to non-stoichiometric magnetite micrograins measuring 100–200 nm, and a structure corresponding to non-stoichiometric pyrrhotite $Fe_{1-x}S$. The spectra also contained paramagnetic doublets of high-spin Fe^{2+} ions and Fe^{3+} ions in the octahedral environment of either the O^{2-} ions or the hydroxyl groups, which most probably were distributed throughout the intact COM matrix.

The relationship between the phase composition of iron-containing components and the degree of COM conversion was studied.[242] It was found that an increase in the catalytic activity correlated with an increase in the relative content of metal phase clusters and a decrease in the pyrrhotite cluster content. The interatomic distances between the iron and cobalt ions in the mixed oxide prepared from a bimetallic iron–cobalt acetylacetonate complex were substantially shorter than in the oxide prepared from a mixture of monometallic acetylacetonates. It is because of this that in the former case nanosized intermetallic active components formed, which increased the catalytic activity (Table 5, samples **6** an **7**). In contrast, the use of monometallic

Table 5. Brown coal hydrogenation in tetralin in the presence of mono- and heteronuclear metal-containing complexes (P = 10 MPa, τ = 2 h).

Sample	Applied complex	Metal content (mass %)		T_{exp} / K	COM conversion (%)	Yield of liquid products (%)	Yield of gases (%)	
		Fe	Co				hydrocarbons	$CO + CO_2$
1	without application			653	32.5	27.0	2.8	2.7
2	$Fe(acac)_3$	1.5		653	68.0	56.5	4.5	8.0
3	$Fe(acac)_3$	1.5		693	86.0	59.3	14.7	12.0
5	$Co(acac)_2$		1.5	653	78.0	52.5	14.7	10.8
6	$FeCo_x(acac)_y$	0.45	1.05	653	86.0	61.0	12.5	11.6
7	$FeCo_x(acac)_y$	0.45	1.05	693	90.0	66.1	13.7	10.2
8	$Fe(acac)_3 + Co(acac)_2$	0.45	1.05	653	74.0	46.7	15.9	11.4
9	$Fe(acac)_3 + Co(acac)_2$	0.94	0.56	653	70.0	46.3	12.8	10.9

acetylacetonate complexes as the catalyst precursors led to the formation of non-stoichiometric magnetite and pyrrhotite in place of active metal species. Based on this comparison, it can be concluded that iron–cobalt intermetallic species were resistant against sulfur and oxygen contained in the coal.

The synthesized heterometallic iron–cobalt acetylacetonate complex proved to be a promising precursor of the catalyst used in the processing of a mixture of brown coal with bituminous oil employed as the paste-forming agent. In this case, the conversion of the organic mass of mixed starting components reached 88% at the yield of the liquid hydrocarbon fraction of $\sim$ 65%.

Thus, a series of studies [239–242] demonstrated the high catalytic activity of highly dispersed iron-containing oxide and iron–cobalt intermetallic clusters synthesized from metal oxide precursors and stabilized at the interface of carbon grains and natural inorganic oxide admixtures.

VII. Conclusion

The surveyed studies on mixed copper- and iron-containing catalysts based on oxides of different metals demonstrated considerable progress in the field of heterogeneous catalysis in the past 20 years. Modified procedures of synthesis of such catalysts developed by different authors, particularly, the sol–gel process, made it possible to synthesize materials with catalytic properties comparable and in certain cases exceeding the properties of noble metal-containing catalysts.

The analysis of presented data has shown that the alkoxy methods played a special role in the development of complex metal oxide catalysts. Doping of the oxide matrix with transition metal ions in the stage of gel formation resulted in the appearance of solid solutions of substitution only on the surface of the oxide matrix. To form oxides with the uniform distribution of dopants throughout the bulk, higher calcination temperatures were required. This determined the attractiveness of alkoxy methods for the targeted synthesis of heterogeneous catalysts in which the highly dispersed active sites with the complex structure were distributed over the surface of various carriers.

The use of an alkoxy method that employs phosphorus-containing templates in synthesizing titanate catalysts led to the development of materials with unique properties. Thus the synthesized single-phase oxides $P_xTi_{1-0.75x}O_{2\pm\delta}$ had uniform porosity in addition to the narrow size distribution of micrograins. Moreover, the pore size could be regulated from 2 to 4 nm by changing the molecular volume of the phosphorus-containing precursor. Membranes developed on the basis of these oxides exhibited anisotropy of catalytic properties, which depended on the gaseous substrate flow direction. This allowed a membrane-catalytic diode to be developed on their basis.

To date, the most important problems of heterogeneous catalysis included studies of the polymorphism of active components on the interface with the support and also the cooperative interactions between nanoclusters, including the interactions observed in the course of evolution of catalytic systems. It was shown that many nanostructured metal oxides formed as metastable phases. The phase transformations of active components in catalysts depended on both the synthetic method as a whole (impregnation, co-precipitation, sol–gel process, *etc.*) and numerous reaction parameters (*e.g.*, the type of metal-containing precursors, the nature and structure of supports, the use of templates, *etc.*). Elucidation of the relationship 'catalyst's synthetic method and conditions → catalysts structure → catalytic properties' is undeniably determined by the possibilities of the contemporary research physicochemical methods that make it possible to study the structure of active sites and the reaction mechanisms on the latter.

A series of studies on iron-containing mixed oxides that were crystallographically amorphous in all stages of their formation convincingly demonstrated the prospects of combining spectroscopic and magnetic research methods in studying the catalyst structure. The detailed study of nanostrutured oxides prepared by both the alkoxy methods and the deposition on different substrates brought about the whole series of new materials that proved to be efficient and economic catalysts in processing of coal organic mass to hydrocarbons, formation of alkylaromatic hydrocarbons from CO and H_2, and several other industrial processes.

Among the other results, mention should be made of unusual transformations of nanoclusters containing Pt and Pd that occur in metastable non-equilibrium systems on the alumina surface characterized by the enhanced concentration of defects. It was revealed for the first time that the reduction of aluminium–platinum catalyst afforded intermetallic platinum–aluminium clusters distributed over the oxide matrix surface.

As a whole, the results shown in this review can be considered as a new stage in the targeted synthesis of mixed metal oxide catalysts the defective surface and non-stoichiometric composition of which determine the non-equilibrium phase transformations to afford active components.

References

1. N Ya Turova, E P Turevskaya, V G Kessler, M I Yanovskaya *Chemistry of Metal Alkoxides* (Amsterdam: Kluwer Academic, 2001)
2. G Frenzer, W F Maier *Annu. Rev. Mater. Res.* **36** 281 (2006)
3. D A Ward, E I Ko *Ind. Eng. Chem. Res.* **34** 421 (1995)
4. M A Cauqui, J M Rodríguez-Izquierdo *J. Non-Cryst. Solids* **147 – 148** 724 (1992)
5. M Fernández-Garcia, A Martinez-Arias, J C Hanson, J A Rodríguez *Chem. Rev.* **104** 4063 (2004)
6. I E Wachs *Catal. Today* **100** 79 (2005)
7. K R M Rao, F E Huggins, V Mahajan, G P Huffman, V U S Rao, B L Bhatt, D B Bukur, B H Davis, R J O'Brien *Top. Catal.* **2** 71 (1995)
8. S Li, G D Meitzner, E Eglesia *J. Phys. Chem. B* **105** 5743 (2001)
9. P S Sai Prasad, J W Bae, K-W Jun, K-W Lee *Catal. Surv. Asia* **12** 170 (2008)
10. N D Spencer, R C Schoonmaker, G A Somorjai *J. Catal.* **74** 129 (1982)
11. M Boudart, D G Loffler *J. Phys. Chem.* **88** 5763 (1984)
12. J Sehested, C J H Jacobsen, E Törnqvist, S Rokni, P Stoltze *J. Catal.* **188** 83 (1999)
13. A Corma *Chem. Rev.* **97** 2373 (1997)
14. G Gottardi *Eur. J. Mineral.* **1** 479 (1989)
15. E Coker, J C Jansen, J A Martens, P A Jacobs, F DiRenzo, F Fajula, A Sacco Jr *Micropor. Mesopor. Mater.* **23** 119 (1998)
16. V I Bukhtiyarov, I G Slin'ko *Usp. Khim.* **70** 167 (2001) [*Russ. Chem. Rev.* **70** 147 (2001)]
17. J A Schwarz *Chem. Rev.* **95** 477 (1995)
18. S P Jiang *Mater. Sci. Eng. A* **418** 199 (2006)
19. G A Somorjai, J Y Park *Top. Catal.* **49** 126 (2008)
20. V Meille *Appl. Catal. A* **315** 1 (2006)
21. J E Sunstrom IV, W R Moser, B Marshik-Guerts *Chem. Mater.* **8** 2061 (1996)
22. A G Chakinala, P R Godate, A E Burgess, D H Bremmer *Chem. Eng. J.* **152** 498 (2009)
23. L S Ott, R G Finke *Coord. Chem. Rev.* **252** 1075 (2007)
24. R V Kumar, Y Diamant, A Gedanken *Mater. Chem.* **12** 2301 (2000)
25. RF P. 2234979; *Byull. Isobr.* (24) (2004)
26. U F Zav'yalova, V F Tret'yakov, T N Burdeinaya, V V Lunin, N B Shitova, N D Ryzhova, A N Shmakov, A I Nizovskii, P G Tsyrul'nikov *Kinet. Katal.* **46** 795 (2005) [a]
27. R C Mehrotra, A K Ray *Polyhedron* **10** 1103 (1991)
28. A Pintar, J Batista, S Hocevar *J. Coloids Interf. Sci.* **285** 218 (2005)
29. Y Abe, T Gundji, Y Kimata, M Kuzamator, A Kasaor, T Misonj *J. Non-Cryst. Solids* **121** 21 (1990)
30. D Gamarra, G Munuera, A B Hungria, M Fernández-Garcia, J C Conesa, P A Midgley, X Q Wang, J C Hanson, J A Rodriguez, A Martinez-Arias *J. Phys. Chem. C* **111** 11026 (2007)
31. M Schultz, E Matijević *Colloids Surf. A* **131** 173 (1998)
32. J G Morales, R R Clemente, E Matijeviś *J. Colloid Interf. Sci.* **151** (2) 555 (1992)
33. J Livage *J. Solid State Chem.* **64** 322 (1986)
34. D C Bradley, R C Mehrotra, D P Gau *Metal Alkoxides* (London, New York, San Francisco: Academic Press, 1978)
35. M V Tsodikov, O V Bukhtenko, O G Ellert, V M Shcherbakov D I Kochubey *J. Mater. Sci.* **30** 1087 (1995)
36. O G Ellert, I A Petrunenko, M V Tsodikov, O V Bukhtenko, D I Kochubey, Yu V Maksimov, E L Cumbrera, A Domingez-Rodrigez *J. Sol-Gel Sci. Techol.* **8** 213 (1997)
37. M V Tsodikov, O V Bukhtenko, O G Ellert, V V Markevich, Yu V Maksimov, S M Loktev *Izv. Akad. Nauk, Ser. Khim.* 295 (1991) [b]
38. O G Ellert, I A Petrunnenko, M V Tsodikov, O V Bukhtenko, D I Kochubey, Yu V Maksimov, A Domingez-Rodrigez *J. Mater. Chem.* **6** 207 (1996)
39. W Von Bidell, in *Inaugural — Dissertation*, Stutgardt, 1992, p. 334
40. R Schmid, H Ahamdane, A Mosset *Inorg. Chim. Acta* **190** 237 (1991)
41. I-H Tseng, W-Ch Chang, J C S Wu *Appl. Catal. B* **37** 37 (2002)
42. I-H Tseng, J C S Wu, H Y Chou *J. Catal.* **221** 432 (2004)
43. K Hirano, K Inoue, T Yatsu *J. Photochem. Photobiol. A* **64** 255 (1992)
44. L Yeung, S T Yau, A J Maira, J M Coronado, J Soria, P L Yue *J. Catal.* **219** 107 (2003)
45. P Yang, D Zhao, D I Margoles, B F Chmelka, G D Stucky *Nature (London)* **396** 152 (1998)
46. P Yang, D Zhao, D I Margoles, B F Chmelka, G D Stucky *Chem. Mater.* **11** 2813 (1999)
47. E L Crepaldi, G J A A Soler-Illia, D Crosso, F Cagnol, F Ribot, C Sanchez *J. Am. Chem. Soc.* **125** 9770 (2003)
48. H Fujii, M Ohtaki, K Eguchi *J. Am. Chem. Soc.* **120** 6832 (1998)
49. S Y Choi, M Mamak, N Coombs, N Chopra, G A Ozin *Adv. Funct. Mater.* **14** 335 (2004)
50. G J A A Soler-Illia, E L Crepaldi, D Grosso, D Durand, C Sanchez *Chem. Commun.* 2298 (2002)
51. G J A A Soler-Illia, A Louis, C Sanchez *Chem. Mater.* **14** 750 (2002)
52. D M Antonelli, V Y Ying *Angew. Chem., Int. Ed.* **34** 2014 (1995)
53. G J A A Soler-Illia, C Sanchez, B Lebeau, J Patarin *Chem. Rev.* **102** 4093 (2002)
54. M Cozzolino, M Di Serio, R Tesser, E Santacesaria *Appl. Catal. A* **325** 256 (2007)
55. A D Wadsley, S Andersson *Persp. Struct. Chem.* **3** 1 (1970)
56. M V Tsodikov, E V Slivinskii, V V Yushchenko, L E Kitaev, V V Kriventsov, D I Kochubei, A T Teleshev *Izv. Akad. Nauk, Ser. Khim.* 152 (2000) [b]
57. R A Kozlovskii, V V Yushchenko, L E Kitaev, O V Bukhtenko, A M Voloshchuk, L N Vasil'eva, M V Tsodikov *Izv. Akad. Nauk, Ser. Khim.* 887 (2002) [b]
58. V V Teplyakov, M V Tsodikov, M I Magsumov, F Kaptein *Kinet. Katal.* **48** 139 (2007) [a]
59. I M Kurchatov, N I Laguntsov, M V Tsodikov, A S Fedotov, I I Moiseev *Kinet. Katal.* **49** 120 (2008) [a]
60. H Chun, T Yuchao, T Hongxiao *Catal. Today* **90** 325 (2004)
61. J Araña, C Fernández Rodríguez, O González Díaz, J A Herrera Melián, J Pérez Peña *Catal. Today* **101** 261 (2005)
62. J Araña, J M Doña-Rodríguez, O González Díaz, E Tello Rendón, J A Herrera Melián, G Colón, J A Navío, J Pérez Peña *J. Mol. Catal. A* **215** 153 (2004)
63. C He, Y Xiong, X Zhu *Catal. Commun.* **4** 183 (2003)
64. K Chiang, R Amal, T Tran *Adv. Environ. Res.* **6** 471 (2002)
65. F Boccuzzi, A Chiorino, G Martra, M Gargano, N Ravasio, B Carrozzini *J. Catal.* **165** 129 (1997)
66. J C S Wu, I H Tseng, W-C Chang *J. Nanopart. Res.* **3** 113 (2001)
67. J C S Wu, H-M Lin *Int. J. Photoenergy* **7** 115 (2005)
68. X Bokhimi, O Novaro, R D Gonzalez, T López, O Chimal, A Asomoza, R Gómez *J. Solid State Chem.* **144** 349 (1999)
69. M V Tsodikov, Ye A Trusova, Ye V Slivinskii, G G Hernandez, D I Kochubey, V G Lipovich, J A Navio, in *Studies in Surface and Catalysis* Vol. 118 (Eds B Delmon, J T Yates) (Belgium: Lonvain-la-Neuve, 1998) p. 679
70. E A Trusova, M V Tsodikov, E V Slivinskii, G G Hernandez, O V Bukhtenko, T N Gdanova, D I Kochubey, J A Navio *Mendeleev Commun.* 102 (1998)
71. G A Somorjai, A S Mujumdor, in *Introduction to Surface Chemistry and Catalysis* (New York: Wiley-Interscience, 1994) p. 291
72. W R Moser, K E Connolly *Chem. Eng. J.* **64** 239 (1996)
73. F Boccuzzi, A Chiorino, M Gargano, N Ravasio *J. Catal.* **165** 140 (1997)
74. G L Haller, D E Resasco *Adv. Catal.* **108** 364 (1987)
75. M S Wainwright, D L Trimm *Catal. Today* **23** 29 (1995)
76. Y Okamoto, K Fukino, T Imanaka, S Taranishi *J. Phys. Chem.* **87** 3737 (1983)
77. M G Sanchez, J L Gazquez *J. Catal.* **104** 120 (1987)
78. M S Vong, M A Yates, P Reyes, A Perryman, P A Sermon, in *Proceedings of the 9th International Congress on Catalysis Calgary, 1988* Vol. 2 (Eds M J Phillips, M Ternan) (Ottava: Chem. Institute of Canada, 1988) p. 545
79. F S Delk, A Vanvere *J. Catal.* **85** 380 (1984)

80. V Di Castro, M Gargano, N Ravasio, M Rossi, in *Preparation of Catalysts V* (Eds G Poncelet, P A Jacobs, B Delmon) (Amsterdam: Elsevier, 1991) p. 95
81. J Nakamura, I Nakamura, T T Uchijima, Y Kanai, T Wanabe, M Saito, T Fujitani *Catal. Lett*. **31** 325 (1995)
82. J D Grunwaldt, A M Molenbroek, N Y Topsoe, B S Clausen *J. Catal*. **194** 452 (2000)
83. J R Rostrup-Nielsen *Phys. Chem. Chem. Phys*. **3** 283 (2001)
84. T Fujitani, J Nakamura *Appl. Catal. A* **191** 111 (2000)
85. B L Kniep, T Ressler, A Rabis, F Girgsdies, M Baenitz, F Steglich, R Schlögl *Angew. Chem., Int. Ed*. **43** 112 (2004)
86. M M Günter, T Ressler, B Bems, C Büscher, T Genger, O Hinrichen, M Muhler, R Schlögl *Catal. Lett*. **71** 37 (2001)
87. B Bems, M Schur, A Dasenoy, H Junkes, D Herein, R Schlögl *Chem. – Eur. J*. **9** 2039 (2003)
88. G C Chinchen, K C Waugh, D A Whan *Appl. Catal*. **25** 101 (1986)
89. G C Chinchen, M S Spencer, K C Waugh, D A Whan *J. Chem. Socyu, Faraday Trans*. **83** 2193 (1987)
90. W X Pan, R Cao, D L Roberts, G L Griffin *J. Catal*. **114** 440 (1988)
91. RB Rasmussen, M Kazuta, I C Horkendorff *Surf. Sci*. **318** 267 (1994)
92. P B Rasmussen, P M Holmblad, C V Askgaard, C V Ovesen, P Stoltze, J K Norskov, I Chorkendorff *Catal. Lett*. **26** 373 (1994)
93. T S Askgaad, J K Norskov, C V Ovesen, P Stoltze *J. Catal*. **156** 229 (1995)
94. R G Herman, K Klier, G W Simmons, B P Finn, J B Bulko, T P Kobylinski *J. Catal*. **56** 407 (1979)
95. G R Sheffer, T S King *J. Catal*. **115** 376 (1989)
96. J Szanyi, D W Goodman *Catal. Lett*. **10** 383 (1991)
97. R Burch, R J Chappel, S E Golunski *J. Chem. Soc., Faraday Trans*. **85** 3569 (1989)
98. R Burch, S E Golunski, M S Spencer *J. Chem. Soc., Faraday Trans*. **86** 2683 (1990)
99. R Burch, R J Chappell, S E Golunski *Catal. Lett*. **1** 439 (1988)
100. J Yoshihara, C T Campbell *J. Catal*. **161** 776 (1996)
101. C V Ovesen, B S Clausen, J Schiotz, P Stoltze, H Topsoe, J K Norskov *J. Catal*. **168** 133 (1997)
102. R A Hadden, B Sakakini, J Tabatabaei, K C Waugh *Catal. Lett*. **44** 45 (1997)
103. Y Kanai, T Watanabe, T Fujitani, M Saito, J Nakamura, T Uchijima *Catal. Lett*. **27** 67 (1994)
104. J Nakamura, Y Kanai, T Uchijima, T Fujitani *Catal. Today* **28** 223 (1996)
105. Y Kanai, T Watanabe, T Fujitani, T Uchijima, J Nakamura *Catal. Lett*. **38** 157 (1996)
106. G R Sheffer, T S King *J. Catal*. **116** 488 (1989)
107. J Nakamura, I Nakamura, T Uchijima, Y Kanai, T Watanabe, M Saito, T Fujitani *J. Catal*. **160** 65 (1996)
108. J Nakamura, I Nakamura, T Uchijima, T Watanabe, T Fujitani *11th Int. Congr. Catal., Stud. Surf. Sci. Catal*. **101** 1389 (1996)
109. T Fujitani, I Nakamura, T Uchijima, J Nakamura *Surf. Sci*. **383** 285 (1997)
110. T Fujitani, T Matsuda, Y Kushida, S Ogihara, T Uchijima, J Nakamura *Catal. Lett*. **49** 175 (1997)
111. I Nakamura, Y Nakano, T Fujitani, T Uchijima, J Nakamura *Surf. Sci*. **402 – 404** 92 (1998)
112. I Nakamura, T Fujitani, T Uchijima, J Nakamura *Surf. Sci*. **400** 387 (1998)
113. G C Miller, C H Rochester, K C Waugh *J. Chem. Soc., Faraday Trans*. **88** 1033 (1992)
114. J E Bailie, C H Rochester, G J Millar *Catal. Lett*. **31** 333 (1995)
115. H Praliaud, S Mikhailenko, Z Chajar, M Primet *Appl. Catal. B* **16** 359 (1998)
116. F Radtke, R A Koeppel E G Minardi, A Baiker *J. Catal*. **167** 127 (1997)
117. J B Ko, C M Bae, Y S Jung, D H Kim *Catal. Lett*. **105** 157 (2005)
118. H Yahiro, K Nakaya, T Yamamoto, K Saiki, H Yamaura *Catal. Commun*. **7** 228 (2006)
119. J Agrell, H Birgersson, M Boutonnet, I Melian-Gambrera, R M Navarro, J L G Fierro *J. Catal*. **219** 389 (2003)
120. T W Kim, M W Song, H L Koh, K L Kim *Appl. Catal. A* **210** 35 (2001)
121. Z-Y Ma, C Yang, W Wei, W-H Li, Y-H Sun *J. Mol. Catal. A* **231** 35 (2005)
122. J P Breen, J R H Ross *Catal. Today* **51** 521 (1999)
123. P H Matter, D J Braden, U S Ozkan *J. Catal*. **223** 340 (2004)
124. P J Wild, M J F M Verhaak *Catal. Today* **60** 3 (2000)
125. S Velu, K Suzuki, M Okazaki, M P Kaqpoor, T Ozaki, F Ohashi *J. Catal*. **194** 373 (2000)
126. A Saadi, Z Rassoul, M M Bettahar *J. Mol. Catal. A* **164** 205 (2000)
127. R Rao, A Dandekar, R T K Baker, M A Vannice *J. Catal*. **171** 406 (1997)
128. K V R Chary, G V Sagar, C S Srikanth, V V Rao *J. Phys. Chem. B* **111** 543 (2007)
129. M T Fabina, M Schmal *Appl. Catal. A* **163** 153 (1997)
130. V Z Fridman, A A Davydov *J. Catal*. **195** 20 (2000)
131. K Chen, S Xie, E Iglesia, A T Bell *J. Catal*. **189** 421 (2000)
132. E E Ortelli, J Wambach, A Wokaun *Appl. Catal. A* **216** 227 (2001)
133. K Tanabe, T Yamaguchi *Catal. Today* **20** 185 (1994)
134. T Yamaguchi *Catal. Today* **20** 199 (1994)
135. I A Fisher, A T Bell *J. Catal*. **172** 222 (1997)
136. F Arena, K Barbera, G Italiano, G Bonura, L Spadaro, F Fruster *J. Catal*. **249** 185 (2007)
137. A S Lisityn, V L Kuznetsov, V L Yermakov *React. Kinet. Catal. Lett*. **14** 445 (1980)
138. L A Bruce, G H Hope, J F Matthews *Appl. Catal*. **8** 349 (1983)
139. H Miyata, S Tokuda, T Ono, T Ohno, F Hatayama *J. Chem. Soc., Faraday Trans*. **86** 2291 (1990)
140. D Kulkarni, I E Waches *Appl. Catal. A* **237** 121 (2002)
141. M L Cubeiro, J L Fierro *Appl. Catal. A* **168** 307 (1998)
142. L J Burcham, I E Waches *Catal. Today* **49** 467 (1999)
143. M Ilyas, Ikramullah *Catal. Commun*. **5** 1 (2004)
144. R A Koppel, C Stocker, A Baiker *J. Catal*. **179** 515 (1998)
145. K T Jung, A T Bell *Catal. Lett*. **80** 63 (2002)
146. M D Rhodes, A T Bell *J. Catal*. **233** 198 (2005)
147. M D Rhodes, K A Pokrovski, A T Bell *J. Catal*. **233** 210 (2005)
148. S Chang, R Doong *Chem. Mater*. **17** 4837 (2005)
149. M C Muoz, S Gallego, J I Beltrán, J Cerdv *Surf. Sci. Rep*. **61** 303 (2006)
150. Z Y Ma, C Yang, W Wei, W H Li, Y H Sun *J. Mol. Catal., A* **231** 75 (2005)
151. Y Zhao, K Nao, H L Wan *Catal. Commun*. **5** 249 (2004)
152. R A Koeppel, A Baiker, A Wokaun *Appl. Catal. A* **84** 77 (1992)
153. L-C Wang, Q Liu, M Chen, Y-M Liu, Y Cao, H-Y He, K-N Fan *J. Phys. Chem. S* **111** 16549 (2007)
154. M Li, Z Feng, G Xiong, P Ying, Q Xin, C Li *J. Phys. Chem. B* **105** 8107 (2001)
155. A A Mirzaei, H R Shaterian, M Habibi, G J Hutchings, S H Taylor *Appl. Catal. A* **253** 499 (2003)
156. M Krämer, T Schmidt, K Stöwe, W F Maier *Appl. Catal. A* **302** 257 (2006)
157. M Kang, E D Park, J M Kim, J E Yie *Catal. Today, B* **111** 236 (2006)
158. Y Tanaka, T Utaka, R Kikuchi, T Takeguchi, K Sasaki, K Eguchi *J. Catal*. **215** 271 (2003)
159. M R Morales, B P Barbero, L E Cadús *Appl. Catal. B* **67** 229 (2006)
160. F Wang, G Yang, W Zhang, W Wu, J Xu *Chem. Commun* 1172 (2003)
161. F Wang, G Yang, W Zhang, W Wu, J Xu *Adv. Synth. Catal*. **346** 633 (2004)
162. Y F Han, K Ramesh, L W C Chen, S Chilukoti, E Widjaja, F X Chen *J. Phys. Chem. C* **11** 2830 (2007)
163. K Ramesh, L W Chen, F X Chen, Z Y Zhong, J H Chin, H W Mook, Y F Han *Catal. Commun*. **8** 1421 (2007)
164. Y F Han, F X Chen, Z Y Zhong, K Ramesh, L W Chen, J H Chin, E Widjaja *J. Phys. Chem. B* **110** 24450 (2006)

165. J Papavasiliou, G Avgouropoulos, T Ioannides *Appl. Catal. B* **66** 168 (2006)
166. J Papavasiliou, G Avgouropoulos, T Ioannides *J. Catal.* **251** 7 (2007)
167. J Papavasiliou, G Avgouropoulos, T Ioannides *Catal. Commun.* **6** 497 (2005)
168. I Spassova, M Khristova, D Panayotov, D Mehandjiev *J. Catal.* **185** 43 (1999)
169. G Schwab, S Kanungo *J. Phys. Chem.* **107** 109 (1977)
170. Q Liu, L-C Wang, M Chen, Y-M Liu, Y Cao, H-Y He, K-N Fan *Catal. Lett.* **121** 144 (2008)
171. M Salou, F Kooli, Y Kiyozumi, F Mikazumi *J. Mater. Chem.* **11** 1476 (2001)
172. S Kaliaguine, A V Neste, V Szabo, J E Gallot, M Bassir, R Muzuchuk *Appl. Catal. A* **209** 345 (2001)
173. D A Bulushev, L K Minsker, V I Zaikovskii, A Renken *J. Catal.* **193** 145 (2000)
174. V V Boldyrev, K Tkacova *J. Mater. Synth. Process.* **8** 121 (2000)
175. A Tschöpe, W Liu, M Flitzani-Stephanopoulos, J Y Ying *J. Catal.* **157** 42 (1995)
176. A Pintar, J Batista, S Hocevar *J. Colloid Interface Sci.* **307** 145 (2007)
177. D H Kim, J E Cha *Catal. Lett.* **86** 107 (2003)
178. G Sedmak, S Hočevar, J Levec *J. Catal.* **222** 87 (2004)
179. G Sedmak, S Hočevar, J Levec *Top. Catal.* **30**–**31** 445 (2004)
180. M Flytzani-Stephanopoulos *MRS Bull.* **26** 885 (2001)
181. Y Li, Q Fu, M Flytzani-Stephanopoulos *Appl. Catal. B* **27** 885 (2000)
182. H Kušavar, S Hočevar, J Levec *Appl. Catal. B* **63** 194 (2006)
183. T Tabakova, F Boccuzzi, M Manzoli, J W Sobczak, V Idakiev, D Andreeva *Appl. Catal. A* **298** 127 (2006)
184. S Hočevar, J Batista, J Levec *J. Catal.* **184** 39 (1999)
185. S Hočevar, U Opara Krašovec, B Orel, A S Aricó, H Kim *Appl. Catal. B* **28** 113 (2000)
186. P Bera, K R Priolkar, P R Sarode, M S Hegde, S Emura, R Kumashiro, N P Lalla *Chem. Mater.* **14** 3591 (2002)
187. X Wang, J A Rodriguez, J C Hanson, D Gamarra, A Martínez-Arías, M Fernández-García *J. Phys. Chem. B* **109** 19595 (2005)
188. G Avgouropoulos, T Ioannides, H Matralis *Appl. Catal. B* **56** 87 (2005)
189. X Tang, B Zhang, Y Li, Y Xu, Q Xin, W Shen *Appl. Catal. A* **288** 116 (2005)
190. W Liu, M Flutzani-Stephanopoulos *J. Catal.* **153** 304 (1995)
191. G Sedmak, S Hocevar, J Levec *J. Catal.* **213** 135 (2003)
192. G Avgouropoulos, T Ioannides, H Matralis *Catal. Lett.* **73** 33 (2001)
193. W Liu, M Flitzani-Stephanopoulos, in *Environmental Catalysis (ACS Symp. Ser.)* Vol. 552, Ch. 31 (Ed. J N Armor) (Washington, DC: American Chemical Society, 1994) p. 375
194. W Liu, A F Sarofim, M Flitzani-Stephanopoulos *Appl. Catal. B* **4** 167 (1994)
195. P Zhu, J Li, Q Huang, S Yan, M Liu, R Zhou *J. Nat. Gas Chem.* **18** 346 (2009)
196. V P Pakharukov, E M Moroz, V V Kriventsov, D A Zyuzin, G R Kosmambetova, P E Striznak *Appl. Catal. A* **365** 159 (2009)
197. E Moretti, L Storaro, A Talon, R Moreno-Tost, E Rodríguez-Castellón, A Jiménez-López, M Lenarda *Catal. Lett.* **129** 323 (2009)
198. E Moretti, M Lenarda, L Storaro, A Talon, R Frattini, S Polizzi, E Rodríguez-Castellón, A Jiménez-López *Appl. Catal. B* **72** 149 (2007)
199. E Moretti, M Lenarda, L Storaro, A Talon, T Montanari, G Busca, E Rodríguez-Castellón, A Jiménez-López, M Tureo, G Bagnasco, R Frattini *Appl. Catal. A* **335** 46 (2008)
200. Y-M Liu, L-C Wang, M Chen, J Xu, Y Cao, H-Y He, K-N Fan *Catal. Lett.* **130** (3–4) 350 (2009)
201. A Hornés, D Gamarra, G Munuera, A Fuerte, R X Valenzuela, M J Escudero, L Daza, J C Conesa, P Bera, A Martínez-Arias *J. Power Sources* **192** 70 (2009)
202. X Zhong, J Zhu, J Liu *J. Catal.* **236** 9 (2005)
203. A Pietraszek, P Da Costa, R Marques, P Kornelak, T W Hansen, O J Camra, M Najbar *Catal. Today* **119** 187 (2007)
204. J H Kang, L D Menard, R G Nuzzo, A I Frenkel *J. Am. Chem. Soc.* **128** 12068 (2006)
205. F A Yandieva, M V Tsodikov, A V Chistyakov, V Ya Kugel', Ya V Zubavichus, A A Veligzhanov, L E Kitaev, V V Yushchenko, A E Gekhman, I I Moiseev *Kinet. Katal.* **51** 572 (2010) [a]
206. V K Duplyakin, A S Belyi, N M Ostrovskii, M D Smolikov, E M Chelganov, A I Nizovskii *Dokl Akad. Nauk* **305** 648 (1989) [c]
207. V A Matyshak, T I Khomchenko, N K Bondareva, V I Panchishnyi, V N Korchak *Kinet. Katal.* **39** 100 (1998) [a]
208. A S Belyi *Kinet. Katal.* **46** 728 (2005) [a]
209. J H Kwark, J Hu, D Mei, Ch-W Yi, D H Kim, Ch H F Peden, L F Allard, J Szanyi *Science* **325** 1670 (2009)
210. O P Tkachenko, A Yu Stakheev, L M Kustov, I S Mashkovsky, M van den Berg, W Grunert, N Yu Kozitsyna, S E Nefedov, Zh V Dobrokhotova, V I Shilov, M N Vargaftik, I I Moiseev *Catal. Lett.* **112** 155 (2006)
211. I S Mashkovsky, A Yu Stakheev, M N Vargaftik, O P Tkachenko, G N Bayeva, N Yu Kozitsyna, M van den Berg, W Grunert, I I Moiseev, in *Proceedings of the 9th European Congress Catalysis. EUROPACAT IX, Salamanka, Spain, 2009* p. 10
212. M V Tsodikov, Doctoral Thesis in Chemical Sciences, A V Topchiev Institute of Petrochemical Synthesis, Russian Academy of Sciences, Moscow, 1992
213. M V Tsodikov, Yu V Maksimov, V Ya Kugel, O G Ellert, O V Bukhtenko *J. Catal.* **148** 113 (1994)
214. Yu V Maksimov, I P Suzdalev, M V Tsodikov, V Ya Kugel, O V Bukhtenko, E V Slivinskii, J A Navio *J. Mol. Catal. A* **105** 167 (1996)
215. M V Tsodikov, V Ya Kugel', Yu V Maksimov, T N Zhdanova, G A Kliger, T S Vinogradova, D I Kochubei *Neftekhimiya* **34** 202 (1994) [d]
216. V Ya Kugel, M V Tsodikov, G N Bondarenko, Ye V Slivinskii, D I Kochubey, M C Hidalgo, J A Navio *Langmuir* **15** 463 (1999)
217. M V Tsodikov, V Ya Kugel, E V Slivinskii, G N Bondarenko, Yu V Maksimov, M A Alvarez, M C Hidalgo, J A Navio *Appl. Catal. A* **193** 237 (2000)
218. O S Morozova, Yu V Maksimov, D P Shashkin, P A Shiryaev, V A Zorin, O V Krylov, G N Krjukova *Appl. Catal.* **78** 227 (1991)
219. A N Gritscov, V A Shvets, V B Kazansky *Chem. Phys. Lett.* **35** 511 (1975)
220. Yu V Maksimov, V V Matveev, I P Suzdalev, M V Tsodikov, O G Ellert *Hyperfine Interact.* **57** 1983 (1990)
221. Yu V Maksimov, M V Tsodikov, O V Bukhtenko, O G Ellert, V V Matveev *J. Catal.* **148** 119 (1994)
222. Ch-Y Wang, C Böttcher, D W Bahnemann, J K Dohrmann *J. Mater. Chem.* **13** 2322 (2003)
223. V Kesavan, D Dyar, Y Koltypin, N Perkas, O Palchik, A Gedanken, S Chandrasekaran *J. Indian Inst. Sci.* **82** 113 (2002)
224. X Cao, Y Koltypin, R Prozorov, G Kataby, A Gedanken *J. Mater. Chem.* **7** 2447 (1997)
225. Y Wang, X Tang, L Yin, W Huang, Y Rosenfeld Hacohen, A Gedanken *Adv. Mater.* **12** 1183 (2000)
226. S T Murahashi, Y Oda, T Naota *J. Am. Chem. Soc.* **114** 7913 (1992)
227. M V Tsodikov, T N Rostovshchikova, V V Smirnov, O I Kiseleva, Yu V Maksimov, I P Suzdalev, V N Ikorskii *Catal. Today* **105** 634 (2005)
228. M V Tsodikov, Ya R Katsobashvili, O V Bukhtenko, O G Ellert, V M Novotortsev, in *Fiziko-khimiya Ul'tradispersnykh Sistem (Sbornik)* [Physical Chemistry of Superdispersed Systems (Collection)] (Ed. I V Tananaev) (Moscow: Nauka, 1987) p. 132

229. T N Rostovshchikova, O I Kiseleva, V V Smirnov, Yu V Maksimov, I P Suzdalev, V E Prusakov, M V Tsodikov, V N Ikorskii *Izv. Akad. Nauk, Ser. Khim.* 1705 (2006) [b]
230. T N Rostovshchikova, M V Tsodikov, O V Bukhtenko, V V Smirnov, O I Kiseleva, Yu V Maksimov, D A Pankratov *Izv. Akad. Nauk, Ser. Khim.* 1376 (2005) [b]
231. Yu V Maksimov, I P Suzdalev, V N Ikorskii, O G Ellert, V M Novotortsev, V M Tsodikov, Kh A Navio *Neorg. Mater.* **42** 430 (2006) [e]
232. Yu V Maksimov, M V Tsodikov, M A Perederii, O V Bukhtenko, I P Suzdalev, J A Navio *Surf. Interface Anal.* **30** 74 (2000)
233. V V Smirnov, M V Tsodikov, in *Tezisy Dokladov II Rossiiskoi Konferentsii 'Aktual'nye Problemy Neftekhimii'* (Abstracts of Reports of the Russian Conference 'Actual Problems of Petroleum Chemistry', Ufa, 2005) p. 62
234. M V Tsodikov, V V Teplyakov, A S Fedotov, I M Kurchatov, M S Karaseva, in *Vserossiiskaya Konferentsiya po Novym Problemam Khimicheskoi Fiziki (Tezisy Dokladov)* [All-Russian Conference on Novel Problems of Chemical Physics (Abstracts of Reports), Tuapse, 2007] p. 55
235. Yu V Maksimov, M V Tsodikov, M A Perederii, I P Suzdalev, A I Nekhaev, V T Popov, O V Bukhtenko *Izv. Akad. Nauk, Ser. Khim.* 86 (1997) [b]
236. I V Kalechits *Ros. Khim. Zh. (Zh. Ros. Khim. o-va im. D I Meneleeva)* **29** 63 (1984) [f]
237. B N Kuznetsov *Kataliz Khimicheskikh Prevrashchenii Uglya i Biomassy* (Catalysis Chemical Transformation of Coal and Biomass) (Novosibirsk: Nauka, 1990)
238. F Derbyshire, T Hager *Fuel* **73** 1087 (1994)
239. M V Tsodikov, Yu V Maksimov, O G Ellert, M A Perederii, M M Grozhan *Khim. Tv. Topl.* 96 (1989)
240. M V Tsodikov, M A Perederii, M M Grozhan *Khim. Tv. Topl.* 49 (1990)
241. M V Tsodikov, M A Perederii, O V Bukhtenko, M M Grozhan *Khim. Tv. Topl.* 35 (1989)
242. M V Tsodikov, Yu V Maksimov, G A Teplyakova, M A Perederii, M M Grozhan, S M Loktev *Khim. Tv. Topl.* 92 (1992)

[a] — *Kinet. Catal. (Engl. Transl.)*
[b] — *Russ. Chem. Bull., Int. Ed. (Engl. Transl.)*
[c] — *Dokl. Phys. Chem. (Engl. Transl.)*
[d] — *Petrol. Chem. (Engl. Transl.)*
[e] — *Inorg. Mater. (Engl. Transl.)*
[f] — *Mendeleev Chem. J. (Engl. Transl.)*